

Automated stratigraphic correlation and model building using chronostratigraphic principles

Zoltán Sylvester

*Bureau of Economic Geology, Jackson School of Geosciences, The University of Texas at Austin
@zzsylvester*

This paper is a non-peer reviewed preprint submitted to *EarthArXiv* and has been submitted for publication to a journal for peer review.

AUTOMATED STRATIGRAPHIC CORRELATION AND MODEL BUILDING USING CHRONOSTRATIGRAPHIC PRINCIPLES

PREPRINT, COMPILED AUGUST 6, 2022

Zoltán Sylvester ^{1*}

¹Bureau of Economic Geology, Jackson School of Geosciences, The University of Texas at Austin

ABSTRACT

Note that his manuscript is a preprint and has not been peer-reviewed.

Stratigraphic correlation of geophysical well logs is one of the most important - and most time-consuming - tasks that applied geoscientists perform on a daily basis. Using the dynamic time warping (DTW) algorithm, automated correlation of two wells is a fairly simple task; DTW can also be used to correlate a large number of wells along a single path. However, errors accumulate along a path and loops cannot be closed. To create a three-dimensionally consistent correlation framework, we use a Python implementation of the Wheeler and Hale (2014) approach, which is based on the idea of stretching-an-squeezing all logs into a chronostratigraphic diagram that has relative geologic time (RGT) on its y-axis. The depth shifts needed for the RGT transformation are computed by translating the outputs of a large number of pairwise DTW correlations into a least-squares optimization problem that is solved through the conjugate gradient method. The resulting chronostratigraphic diagram provides an overview of the overall stratigraphy and its variability. To create geologically intuitive well-log cross sections, we use a multi-scale blocking method that relies on the continuous wavelet transform to identify stratigraphic units of a certain scale in one well and then propagate these boundaries to all the other wells. We demonstrate the usefulness of this approach on a dataset with close to 700 wells from the Permian Basin, West Texas. Linear channel bodies in the deepwater Spraberry Formation are easily detected and clearly highlighted in maps and cross sections. The methodology is robust enough for mapping subtle stratigraphic details, previously considered feasible only through manual interpretation. More importantly, it can be used to quickly build three-dimensional stratigraphic models for large segments of sedimentary basins where enough log data is available.

1 INTRODUCTION

Geophysical well logs represent one of the most important types of data used in stratigraphy, sedimentology, and subsurface geoscience. When multiple logs are located relatively close to each other, and they cover the same stratigraphic interval, it is possible to estimate the composition and structure of the subsurface by correlating log samples that are likely to be of the same age. Although three-dimensional seismic reflection surveys provide a more complete picture of the subsurface, well logs have a higher vertical resolution and provide more details about the lithology and depositional facies of the rocks and sediments they penetrate. Correlation of geophysical well logs is one of the most important - and most time-consuming - tasks that applied geoscientists perform on a daily basis. In many onshore- and shallow-water settings, it is common that hundreds or thousands of logs have to be correlated. Doing this manually is time consuming and strenuous; and humans are unable to take advantage of all the stratigraphic information that a dense set of well logs holds. It is obvious that some degree of automation has the potential to substantially decrease the time spent on routine correlation and to increase the reproducibility of the result.

Early attempts to use computers for log correlation have relied on the cross-correlation algorithm to find time-equivalent sample pairs (Rudman and Lankston, 1973; Mann and Dowell, 1978). Later it became obvious that the dynamic time warping (DTW) algorithm handles better logs that differ significantly from each other, a common problem unless the stratigraphy is extremely simple (Lineman et al., 1987; Fang et al., 1992; Zoraster et al., 2004; Hladil et al., 2010; Lallier et al., 2012; Wheeler and Hale, 2014; Wheeler, 2015; Lallier et al., 2016; Grant et al., 2018; Wu et al., 2018). Dynamic time warping has also been used to correlate paleo-proxy records of environmental change (e.g., Lisiecki and Lisiecki, 2002; Lisiecki and Raymo, 2005; Hay et al., 2019; Ajayi et al., 2020). Another line of research takes advantage of neural networks (Baldwin et al., 1989; Luthi and Bryant, 1997; Brazell et al., 2019). The results of Brazell et al. (2019) suggest that the use of deep neural networks for log correlation is a promising approach. Although significant progress has been made in recent years in terms of automation, both with neural networks and the DTW algorithm, the vast majority of log correlation projects still rely on conventional manual interpretation. At the same time, the number of oil and gas wells drilled in onshore basins in the United States has exploded as part of the

*zoltan.sylvester@beg.utexas.edu

shale revolution; in 2019, there were more than 969,000 producing wells in the continental US (EIA, 2020). Many well databases consist of tens of thousands of logs that pose a major challenge to reproducible and efficient manual correlation workflows. These workflows tend to force the interpreter to focus on relatively fine-scale details in a small number of logs and it is difficult and time-consuming to assess the large-scale structure of the subsurface.

There are two end members when it comes to strategies for correlating multiple logs. One approach is to start with one well and propagate the stratigraphic tops from this well to the others following a path. The sequence of wells that defines this path can be optimized so that geological discontinuities like faults are avoided (Wu et al., 2018). The other strategy is to correlate every well pair and then adjust the result so that there are no conflicts between correlations (Wheeler and Hale, 2014). Another important strategic choice is whether a single stratigraphic top is tracked at a time (e.g., Brazell et al., 2019), or large number of tops and therefore the entire stratigraphic framework is created at the same time (Wheeler and Hale, 2014).

In this paper, we describe a quasi-automated approach that builds significantly on previous work but brings together a number of techniques for automation and visualization in a novel way and is designed for working with a large number of well logs and relatively high well density. Important elements include the automated stratigraphic subdivision of logs using the continuous wavelet transform (e.g., Cooper and Cowan, 2009), and adjusting the DTW correlation results by stretching-and-squeezing the logs into a chronostratigraphic diagram, largely following the workflow of Wheeler and Hale (2014). Although the concept of chronostratigraphic diagrams (Wheeler, 1964) and relative geologic time has been fairly widely used in seismic interpretation (de Bruin et al., 2007; Lomask et al., 2009; Qayyum et al., 2014; Wu et al., 2022), it remains underutilized in well log correlation. Our goal here is to demonstrate the potential for rapid and relatively high-quality stratigraphic interpretations when the results of dynamic time warping are transformed into a chronostratigraphic diagram that allows the examination of the large-scale stratigraphic framework early on and also provides the basis for high-resolution correlations that are consistent in three dimensions. We use a large dataset from the Permian Basin in West Texas to illustrate the capabilities and the limitations of this new approach for generating and visualizing stratigraphic frameworks.

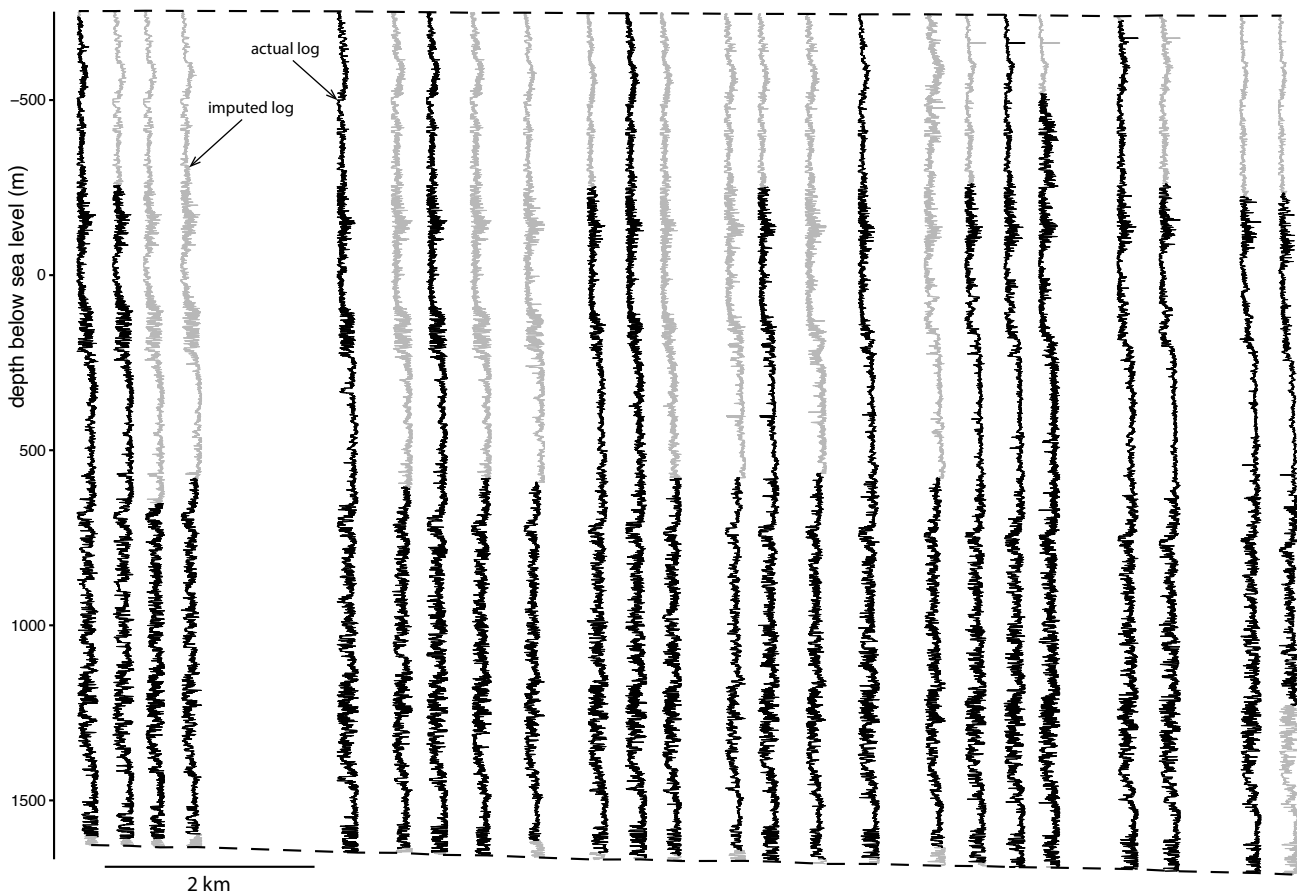


Figure 1: Cross section with a few gamma-ray logs showing the missing, but imputed log segments in gray.

2 METHODS

We have implemented the approach described here as a Python module called ChronoLog that relies on widely used Python packages like numpy (Oliphant, 2006; Harris et al., 2020), scipy (Jones et al., 2001; Virtanen et al., 2020), matplotlib (Hunter, 2007), networkx (Hagberg et al., 2008). Other important packages that ChronoLog uses include librosa (McFee et al., 2015) and verde (Uieda, 2018). All the results and visualizations shown here have been generated through loading and analyzing the well log data in a Jupyter computational notebook environment (Kluyver et al., 2016).

2.1 Data selection and preprocessing

Before loading the log data, decisions have to be made about which logs in the dataset have the quality and quantity to be worth using in the correlation. Although it is possible to use two different types of logs (e.g., gamma ray and density), often logs of a certain type (e.g., gamma ray) are more numerous than other log types, and in this case the results are likely to be better with the larger number of logs as they provide a higher-density coverage of the area of interest. In all wells, an overall top and base depth are required for the interval of interest. These are often not available, especially for a large number of wells; however, in most cases it is sufficient if the missing tops are estimated using a simple interpolation algorithm. Logs with significant missing sections can be either removed; or it is possible to automatically impute the missing upper- and lower parts of such logs if the depth differences between stratigraphically equivalent sections are not too big (Fig. 1).

2.2 Well database / well graph

A special data structure is needed to keep track of all the log data and its spatial context. This is achieved through a Python Well object that contains the name of the well, different types of logs, the corresponding depth values, and the geographic coordinates. Well objects are nodes in a networkx graph and the edges in the graph represent the well pairs (Fig. 2a) that are correlated using the DTW algorithm. DTW correlation results are stored as edge attributes. The advantage of this graph-based approach is that it makes it easy to remove nodes (that is, wells) and/or edges from the database, without compromising data integrity. When a well object is created, the property logs are normalized so that all values are within the 0 to 1 interval, using a lower and upper percentile as the minimum and maximum.

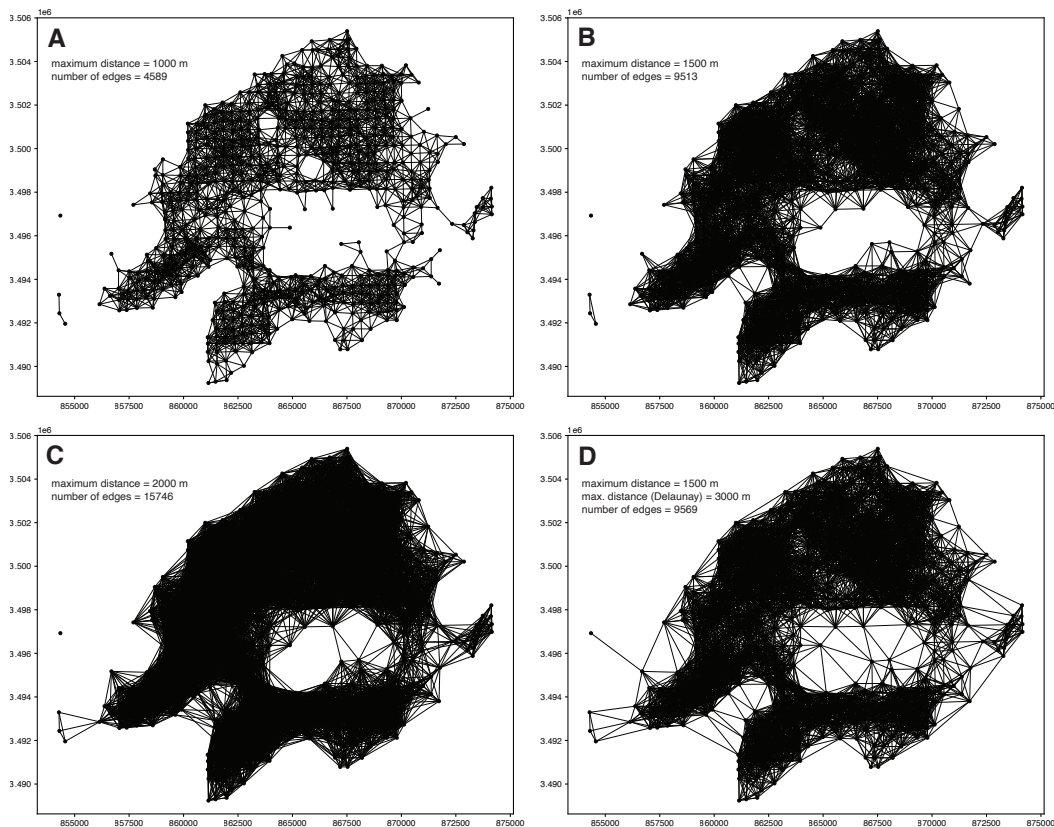


Figure 2: Examples of well graphs for a cluster of wells in the Midland Basin, Texas. Maximum distance is set to (a) 1000 m, (b) 1500 m, (c) 2000 m. In (d) the maximum distance is 1500 m and a Delaunay triangulation is added to connect wells that are farther away from each other.

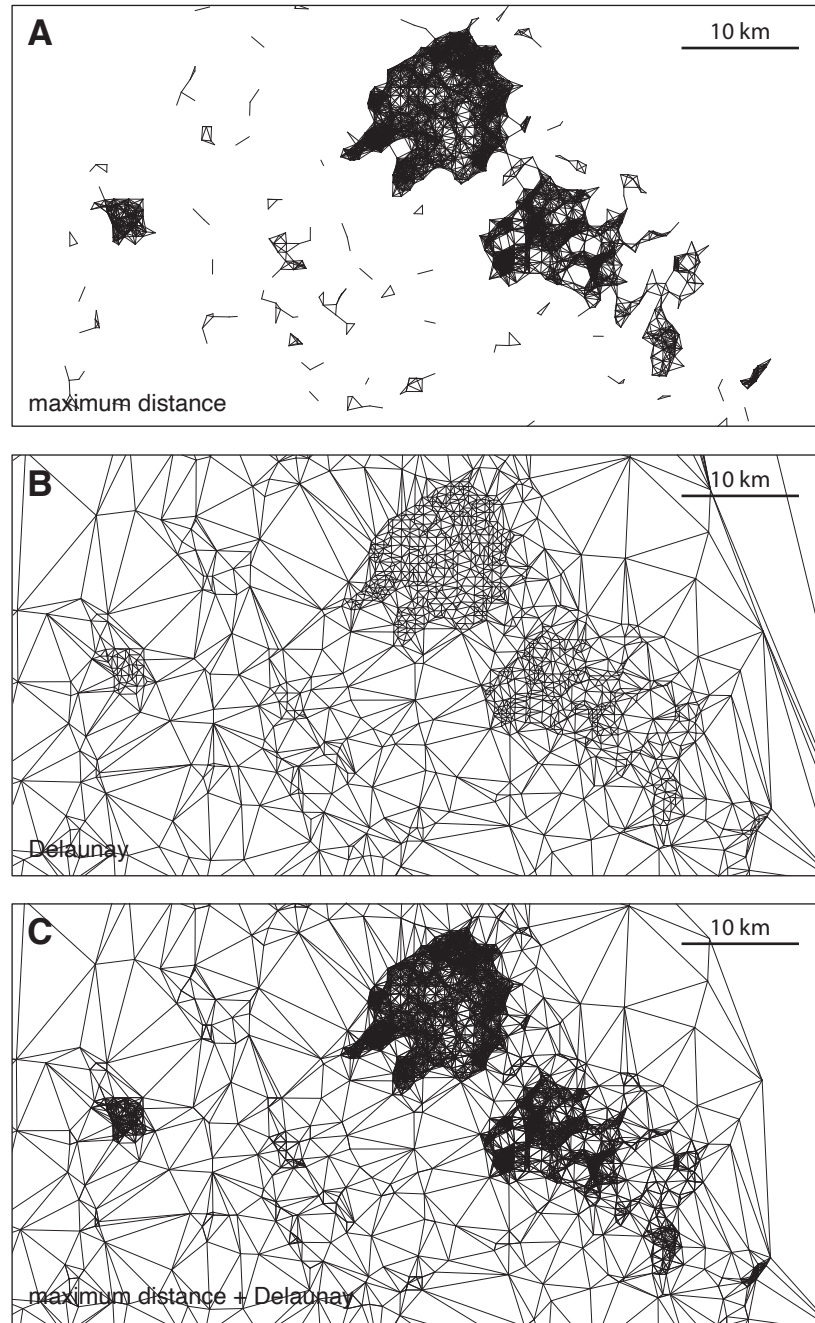


Figure 3: A Delaunay triangulation can be used to connect well clusters and isolated wells. (a) graph only based on maximum distance; (b) Delaunay triangulation; (c) graph that combines the maximum distance graph with the Delaunay triangulation.

2.3 Selection of well pairs to be correlated

The graph is built through adding the well objects as nodes one by one. The number and the identity of the well pairs that will be correlated needs to be decided next. One possibility is to use all the possible well pairs (e.g., Wheeler and Hale, 2014); however, this results in a large number of well pairs even for a limited number of wells. There are 45 well pairs for ten wells; but the number of combinations is 4950 for 100 wells and 499,500 for 1000 wells. The computationally most expensive part of the correlation process is the DTW algorithm, so correlating half a million well pairs requires significant time and/or computational resources. In addition, correlating logs that are far away (e.g., tens of km) from each other tends to decrease the quality of the correlation result. Therefore, a maximum distance parameter is used to define the well pairs, and no edge will be added to the graph if the distance between the wells exceeds this value (Fig. 2).

When the dataset covers a large area, the distribution of wells is often non-uniform as there are clusters of higher well density. To connect all wells, one would need to use a large maximum distance, which would result in an unnecessarily large number of connections in the high-density clusters. We solve this problem by setting the maximum distance to a relatively small number - so that the correlation works well within clusters and there are not too many well pairs - and then connect all the wells through Delaunay triangulation (Fig. 2d, 3). Edges for well pairs that are far away from each other but get connected are removed.

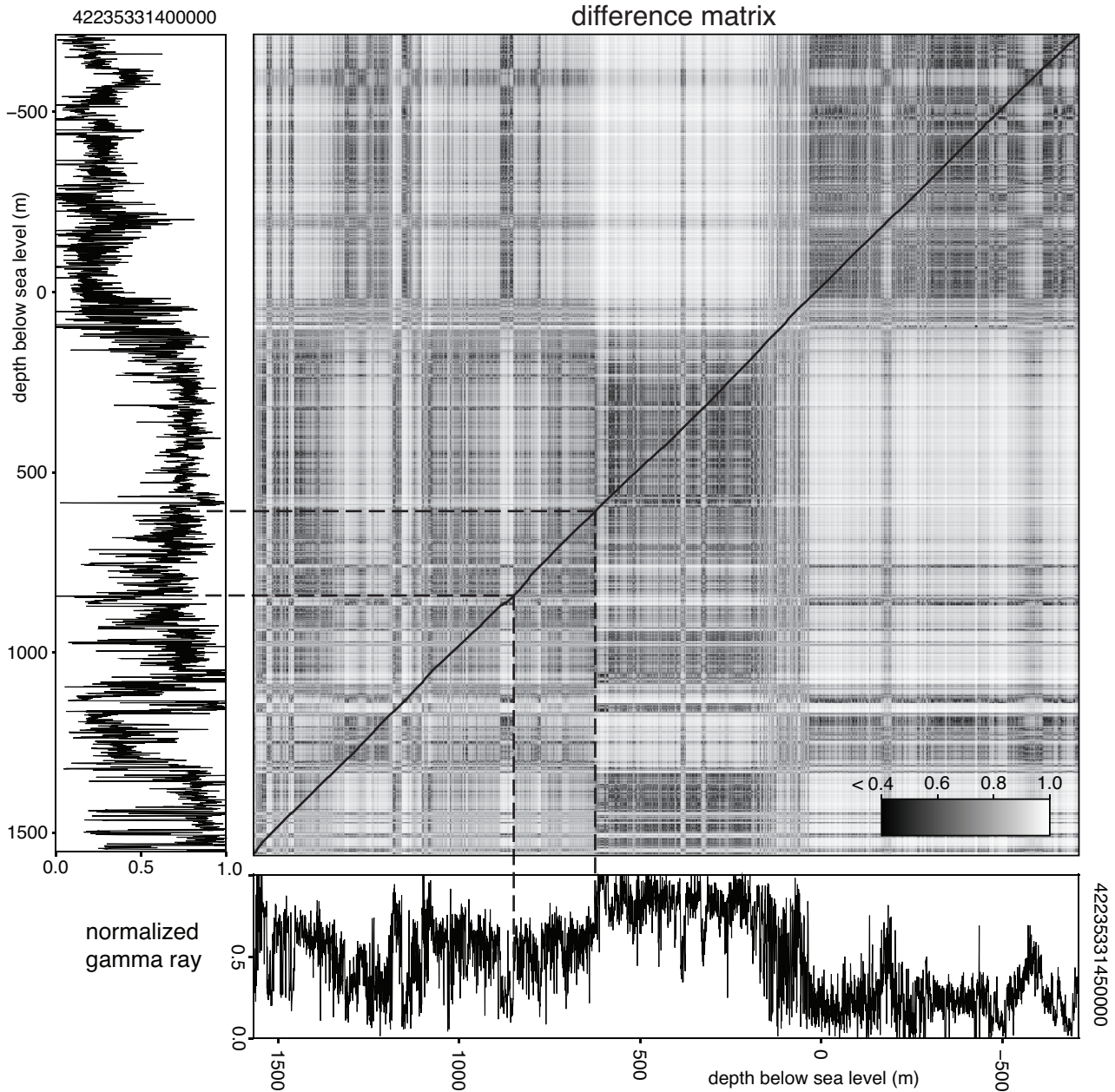


Figure 4: An example of dynamic time warping output: difference matrix and warping path between two gamma-ray logs.

2.4 Well pair correlation using dynamic time warping

After the well pair edges are added to the graph, DTW correlations are performed over all edges and the results are stored as edge attributes. We use the *dtw* function of the *librosa* library (McFee et al., 2015), an implementation that relies on the *numba* package to speed up the computation. This process can be parallelized and significantly sped up if multiple cores are used. Typical run times on a single core are a few minutes for tens of wells, a few tens of minutes to hours for hundreds of wells, and one or more days for thousands of wells. The DTW algorithm finds the optimal correlation between two logs by minimizing the cumulative distance along a correlation path (Figs. 4, 5) and it links every sample in a log to one or more samples in the other

log. The optimal correlation path is computed using a distance matrix (Fig. 4) and a cumulative distance matrix. To visualize the correlation result, it is useful to plot only certain stratigraphic intervals (e.g., defined by a constant step size in the first well) and color them by the average log property (Fig. 5).

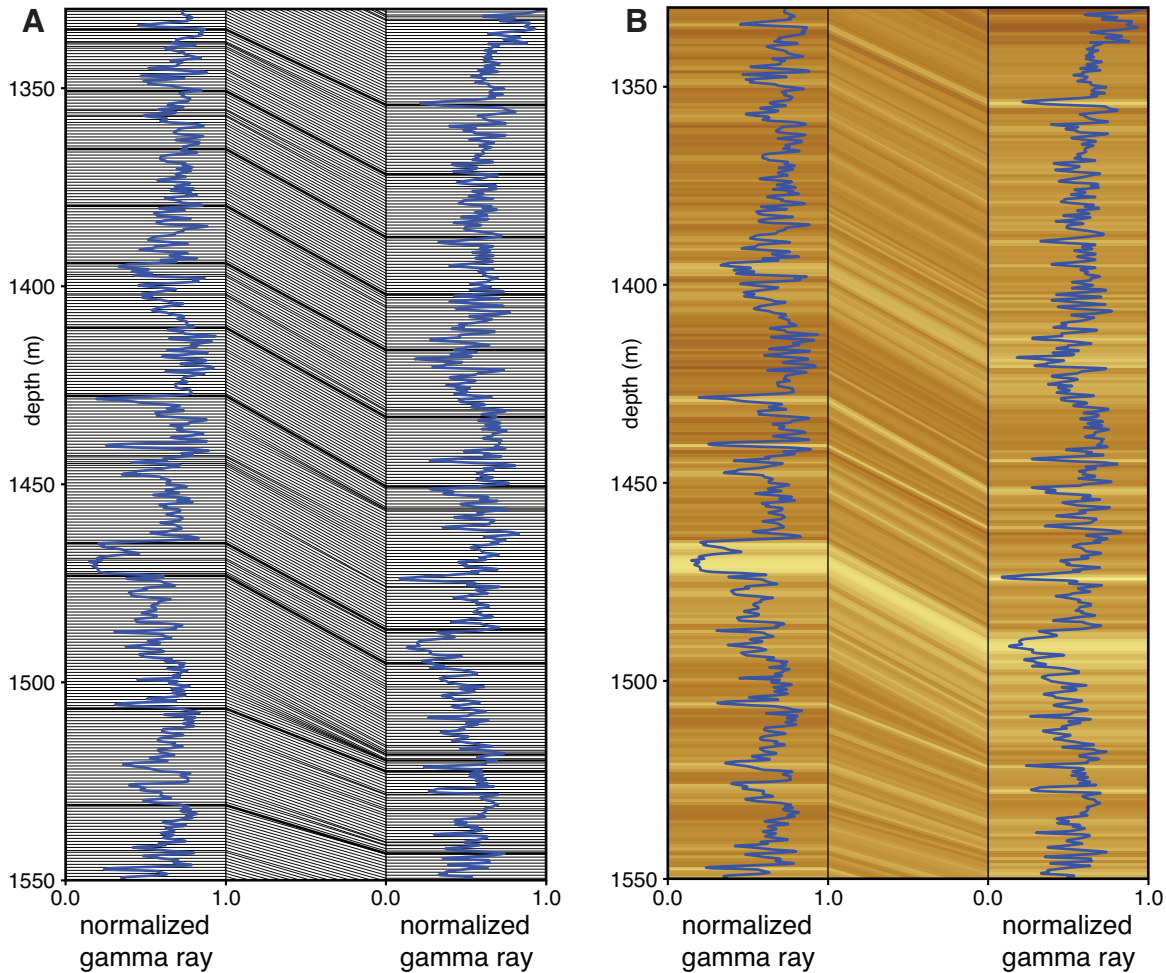


Figure 5: Correlation lines between parts of the logs shown in Fig. 4 (segment between dashed lines in Fig. 4). Only the lines that correspond to every fifth sample in the first log are plotted. A few lines are highlighted for clarity; panel on the right shows how coloring the results by mean log property makes the display more intuitive.

Although it is possible to use DTW to correlate partial sequences, we assume that the first and the last samples in every log pair correlate to each other. The default distance used in the `librosa dtw` function is the Euclidian distance. However, well logs tend to be noisy and the Euclidian distance places too much emphasis on values at the extremities of the distribution; therefore, we use an exponent that is smaller than 1 to reduce the influence of outliers (cf. Wheeler and Hale, 2014):

$$d = |l_2 - l_1|^\alpha, \quad (1)$$

where l_2 and l_1 are the log values and α is the exponent. We have found that 0.15 is a good default value for this parameter.

2.5 Optimization of conflicting pairwise correlations: Chronostratigraphic diagram

Using the pairwise log correlations, it is possible to build correlation panels along any path in the graph, by tracking a stratigraphic top from one log to the next along the path. Although these correlations might look reasonably good at first sight, the correlation errors accumulate from one side of the path to the other and correlation loops cannot be closed, as the vast majority of tops land at different depths in the same well when the path forms a closed loop (Fig. 6). To address this problem and eliminate the correlation conflicts, we stretch-and-squeeze all logs into a chronostratigraphic diagram, with relative geologic time on the y-axis, as suggested by Wheeler and Hale (2014). The key idea is to compute the depth shifts that are applied at every log sample to convert depth to relative geologic time. If two depth values z_1 and z_2 correlate (Fig. 7), it means that the corresponding relative geologic times (RGT) are the same:

$$RGT(z_1) = RGT(z_2) \quad (2)$$

If the depth shifts that are applied to the two samples are s_1 and s_2 , this means that

$$z_1 + s_1 = z_2 + s_2 \tag{3}$$

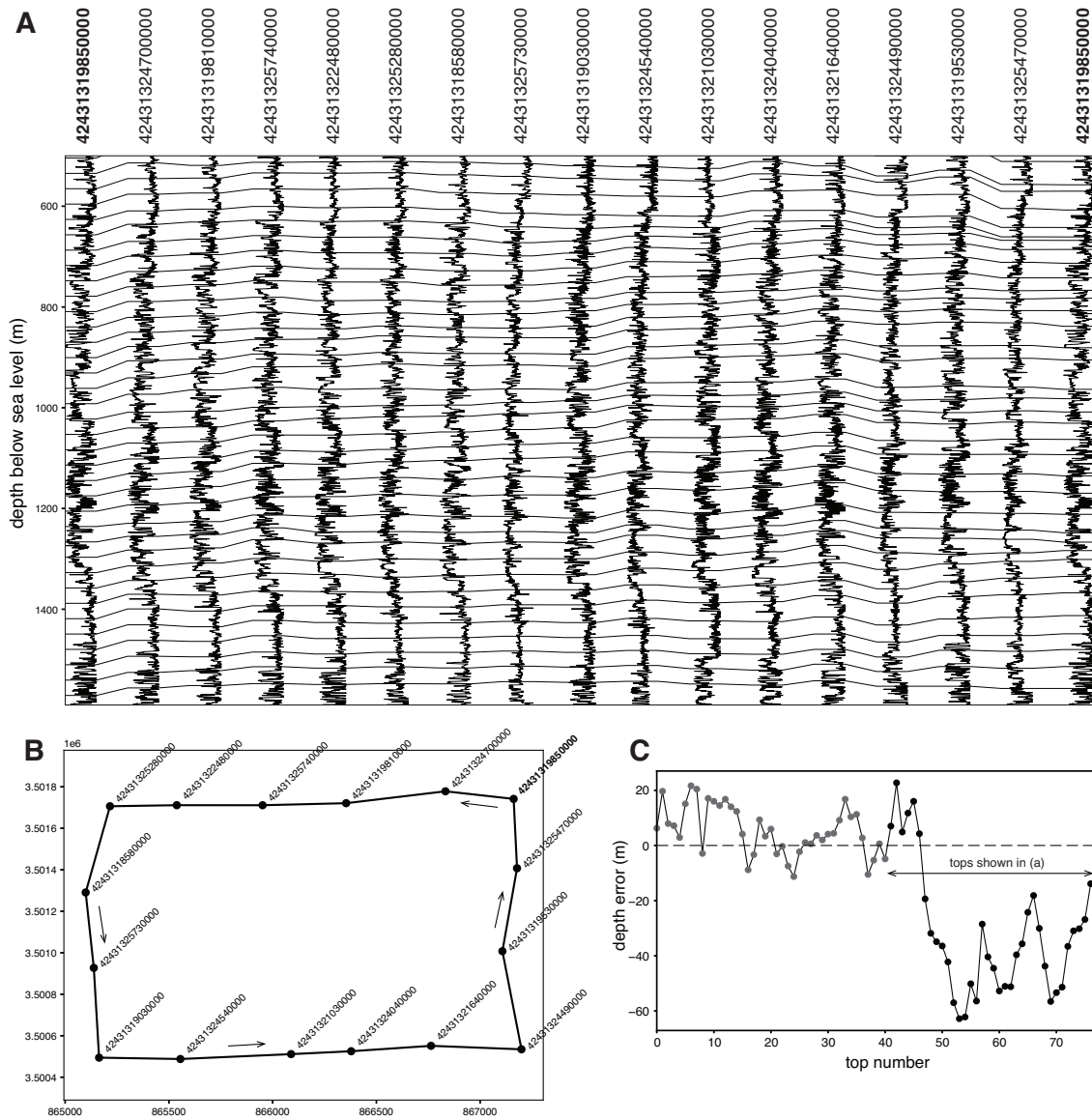


Figure 6: An example of accumulating correlation errors along a correlation path. (a) A loop consisting of 16 wells, where the last log is the same as the first one. A number of equally spaced tops are tracked from the first well; ideally, all the tops should end up at the same depth where they started. That is not the case. (b) Map view of the wells that define the loop. (c) Differences between the starting and ending depths in the first well.

The depth values that correlate are known from the DTW correlations; the shifts are the unknowns. If we bring the unknowns to the left-hand side, we get

$$s_1 - s_2 = z_2 - z_1 \tag{4}$$

An equation like this can be written for every DTW depth pair; in matrix form, the system of equations can be written as

$$D_s s = dz \tag{5}$$

where D_s is the coefficient matrix (that has only values of 1 and -1), s is the array of depth shifts, and dz is the array of depth differences. There is one depth shift for every sample, so the total number of depth shifts is (number of wells) x (number of samples per well). The number of correlated depth pairs is larger than this, as it equals (number of well pairs) x (number of samples per well). This means that the number of equations is larger than the number of unknowns, and there is no exact solution.

A system like this can be treated as a least squares problem (Wheeler and Hale, 2014), and can be solved using the normal equation:

$$D_s^T D_s s = D_s^T dz \tag{6}$$

This is a linear system that has the same number of equations as the number of unknowns (number of samples x number of wells). The coefficient matrix D_s has a size of (number of well pairs x number of samples) x (number of wells x number of samples). This means that, even for a few hundred wells, D_s will have millions of elements and requires a lot of computer memory. The solution to this problem is to avoid creating the whole D_s matrix; instead, we can take advantage of the fact that D_s is a sparse matrix, with nonzero values concentrated along the diagonal.

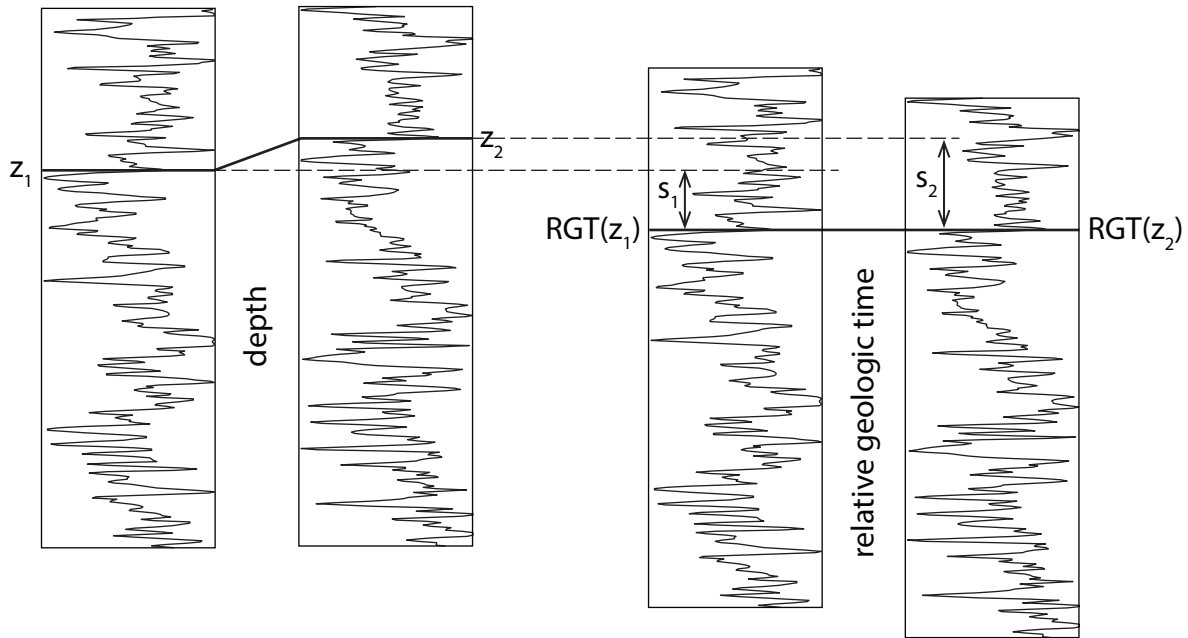


Figure 7: The depth shifts s_1 and s_2 need to be estimated in order to transform the depth values z_1 and z_2 into relative geologic time (RGT). Based on Wheeler and Hale (2014).

Although well logs could be used at their full resolution to compute the depth shifts (Wheeler and Hale, 2014), the computation can be sped up significantly if the logs are resampled to the same - and relatively small - number of samples. Once the shifts are computed at this lower resolution, they are resampled back to the original log resolution so that the shifts have the same number of samples as the other logs from the same well. It would be possible to solve system (6) by solving separately parts that correspond to blocks of nonzero coefficients, as they are independent of each other; however, it is computationally simpler and faster to solve it as one large system, using the conjugate gradient method (Kiusalaas, 2013; Wheeler and Hale, 2014).

To avoid forming the D_s matrix in memory, we assume that depth differences that correspond to a certain starting index in each well pair can be used to estimate the shifts at the same index in both wells. We do this despite the fact that sometimes the second index that is closest to the correlated depth is different from the index in the first well. This simplified approach gives slightly different results from the one with precise indexing; but there is no obvious decrease in the quality of the correlation framework and there are significant savings in computational time and load. Using precise indexing would be more important in situations where the logs are highly similar to each other; in typical geophysical well log pairs, strictly relying on correlations of large- or small values tends to lead to correlation errors.

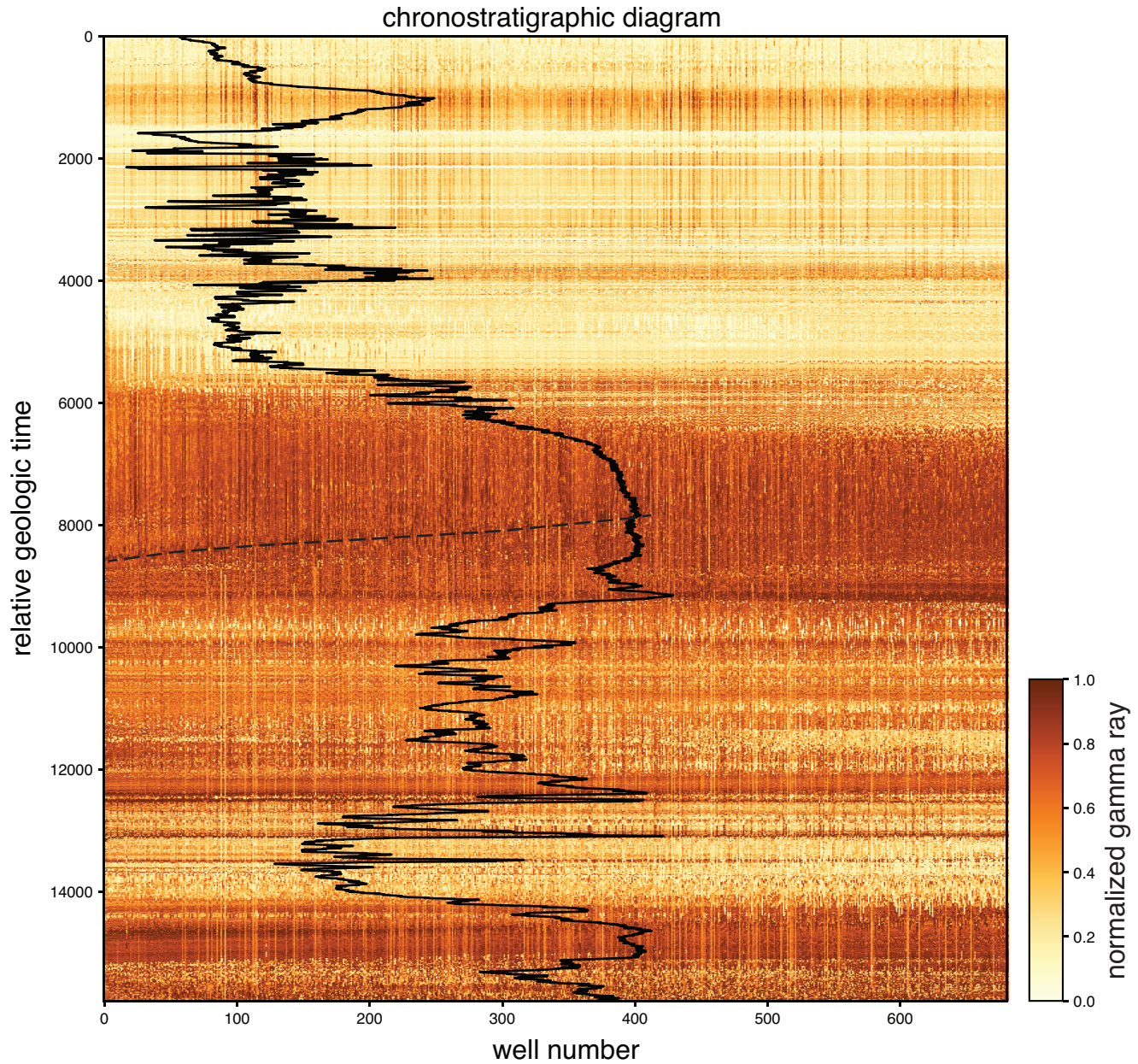


Figure 8: A chronostratigraphic diagram for 681 gamma-ray logs from the Midland Basin, Texas. Black line is the mean normalized gamma ray value for all logs. Dashed line marks the likely location of a clinoform that has not been 'flattened' enough in the correlation process.

After the depth shifts are computed, each log can be converted to RGT space:

$$RGT(z) = z + s \quad (7)$$

If the RGT-transformed logs are resampled to the same length and displayed side-by-side, the result is an image that is also a chronostratigraphic diagram (Fig. 8). In ChronoLog, the default ordering of the logs in this diagram is west to east; but any orientation can be specified through two wells as input parameters. An average well log curve - a type log - can be derived in RGT space by computing the mean of the log values along the horizontal direction (Fig. 8).

A chronostratigraphic diagram built this way gives a high-level overview of the stratigraphy of the area and interval of interest; laterally continuous mudstones are evident, as well as likely facies transitions and possible problem areas where the correlation did not work well. The chronostratigraphic diagram can also be used to manually adjust correlations that appear to be incorrect, for example, when a lithologic marker such as a high-gamma-ray mudstone is vertically offset in places (dashed line in Fig. 8).

2.6 *No going back in time*

The process for estimating depth shifts can result in RGT series that are not entirely monotonic, that is, the principle of superposition might not be always satisfied. This is especially common when significant thickness changes are present in the section of interest. Left uncorrected, these intervals cause problems in the stratigraphic framework and the errors are obvious in cross sections. To avoid such errors, every RGT log is checked for reversals in time and any such reversal is removed through setting the value of the interval that is older than the youngest age in the series so far to that youngest age (Fig. 9). As a result, these intervals have a constant RGT value and can be interpreted as having large relative sedimentation rates compared to the time-equivalent interval in other parts of the area of interest.

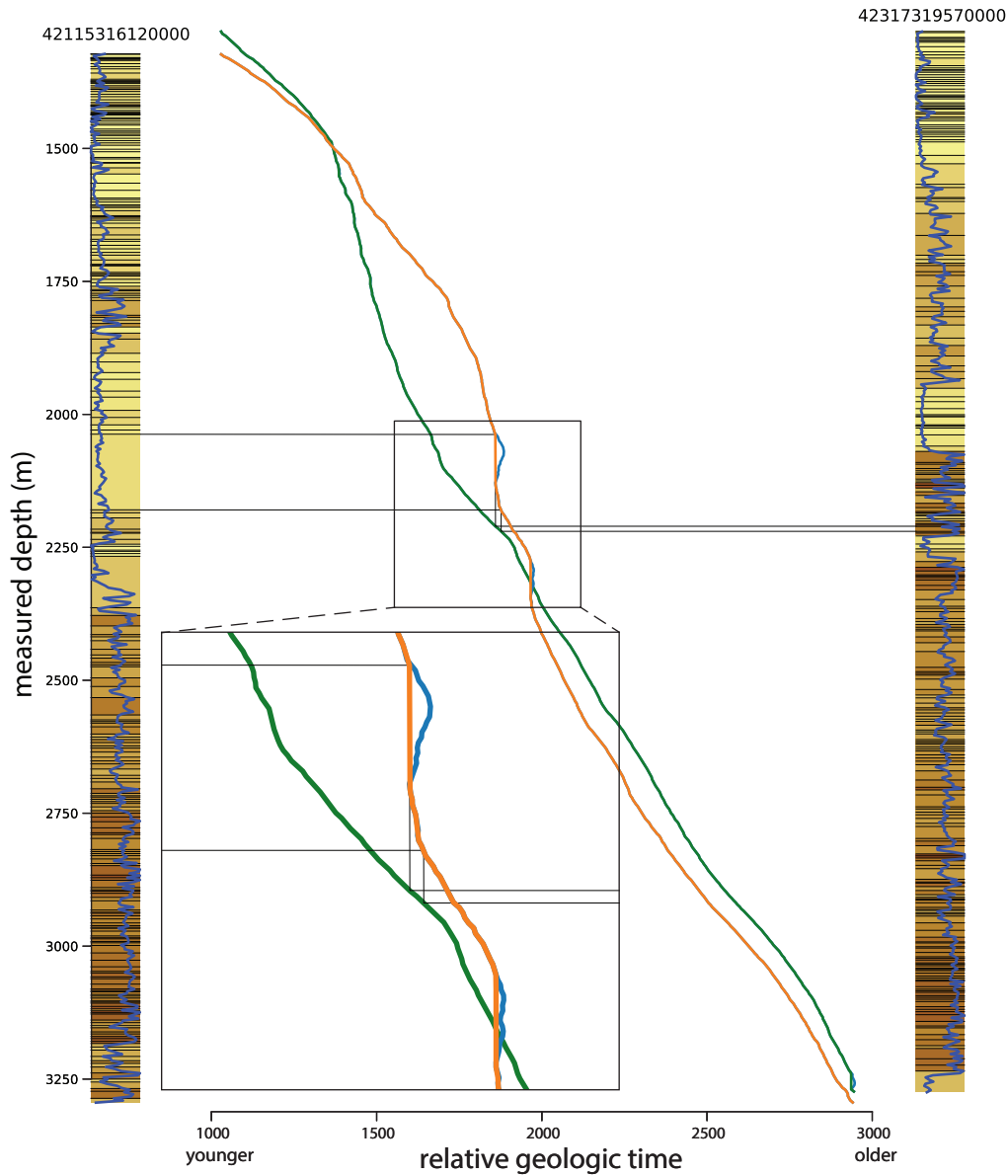


Figure 9: An example RGT log with two depth intervals where the initial RGT curve is decreasing upward (blue curve). In the orange curve, these segments of 'going back in time' are eliminated. As a result, correlations between the two logs become unambiguous and a thick section in the log on the left corresponds to a thin unit on the right. Green curve is the RGT curve for the log on the right.

2.7 *Multi-scale subdivision of logs using the continuous wavelet transform*

So far, the main output of the ChronoLog process is a chronostratigraphic diagram, in which every horizontal line is a correlation line. To preserve as much detail as possible, the RGT logs are resampled at a resolution similar to the log resolution; and as a result, there is a large number - usually hundreds to thousands - of potential stratigraphic tops. Significant surfaces can be selected

manually from the diagram; but this can be a subjective and time-consuming process. Therefore, we use a continuous wavelet transform (CWT), applied to the type log derived from the chronostratigraphic diagram, to automatically define stratigraphic tops at different scales (Cooper and Cowan, 2009; Fig. 10). Ricker wavelets of different dominant frequencies are convolved with the well log and the outputs are stacked, starting from high- to low frequencies. For a given scale / frequency, stratigraphic tops can be obtained through finding the zero values of the corresponding CWT and tracing them back to the highest frequency on the left (Fig. 10). This way, the section of interest can be subdivided into multiple stratigraphic intervals of different scales; in addition, larger-scale stratigraphic tops are subsets of higher-resolution sets. In other words, this is a quick and reproducible way to generate a multi-scale stratigraphic hierarchy with the desired number of hierarchical levels; and applying this method to the average log of the whole dataset means that the higher-level tops have a dataset-wide significance.

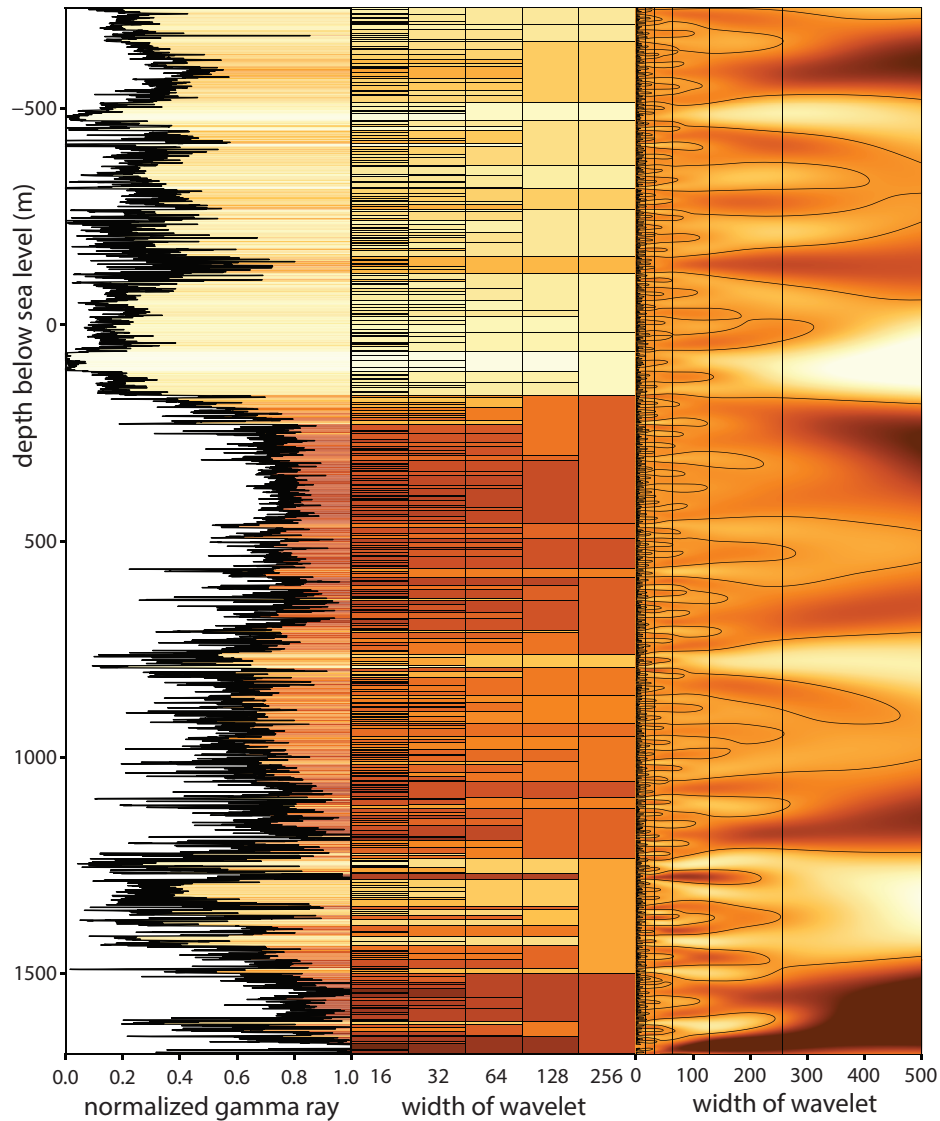


Figure 10: The continuous wavelet transform is used to define multi-scale stratigraphic subdivisions of a gamma-ray log. Continuous wavelet transform panel shown on the right, stratigraphic hierarchy in the middle.

2.8 Converting tops from RGT to depth and visualization in depth

Using the chronostratigraphic diagram and the continuous wavelet transform, we are able to select stratigraphic tops at different scales. However, these are still in RGT space and need to be converted to depth:

$$z = RGT(z)_{min} + i * dz - s, \tag{8}$$

Where z is depth, $RGT(z)_{min}$ is the minimum RGT value for the log of interest, i is the index array of the chronostratigraphic diagram, dz is the sampling rate of the chronostratigraphic diagram, and s is the sequence of depth shifts. If the depth arrays

calculated this way are stacked into an array of the same dimensions as the chronostratigraphic diagram, any stratigraphic top can be quickly extracted by finding the corresponding row in this depth array.

Using stratigraphic tops defined at a certain scale, it is possible to generate cross sections from any sequence of wells. To make these sections geologically more intuitive, every stratigraphic interval (defined by two tops) at a well location is colored by the average log property. Between two consecutive wells in a section, connecting layers are colored by the average properties of the interval in the two wells (Fig. 12).

2.9 Build 3D stratigraphic model

Because every stratigraphic top is defined at every well location, if the well density is high enough, it is possible to inter- and extrapolate depth values and log properties away from the wells and create regularly gridded maps. We use the Python package verde for this purpose; verde relies on Greens functions to grid sparsely and unevenly sampled spatial data (Uieda, 2018). ChronoLog includes functions for creating both structure maps (defined by one stratigraphic top) and property maps (defined by two stratigraphic tops).

Gridding all stratigraphic tops and gridding the mean property values between them makes it possible to build three-dimensional models that are regularly gridded in x-y space and match the stratigraphic boundaries at the wells. These models can be coarsened or refined to the resolution that is required for a particular problem, using the stratigraphic hierarchy created during the correlation process. The grid coarsening will automatically keep the important stratigraphic boundaries in place, as this is how the hierarchy was defined initially.

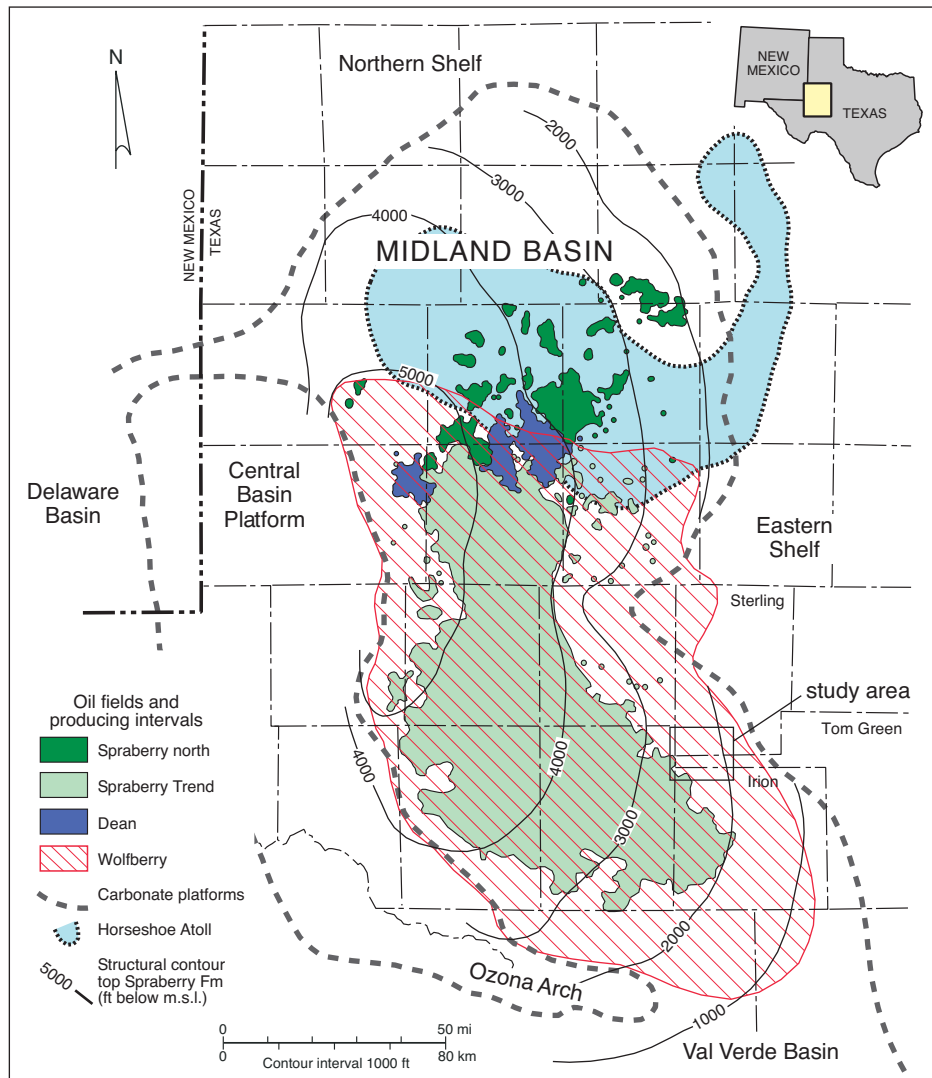


Figure 11: Location of the study area in the Midland Basin, Texas (from Hamlin and Baumgardner, 2012; used with permission).

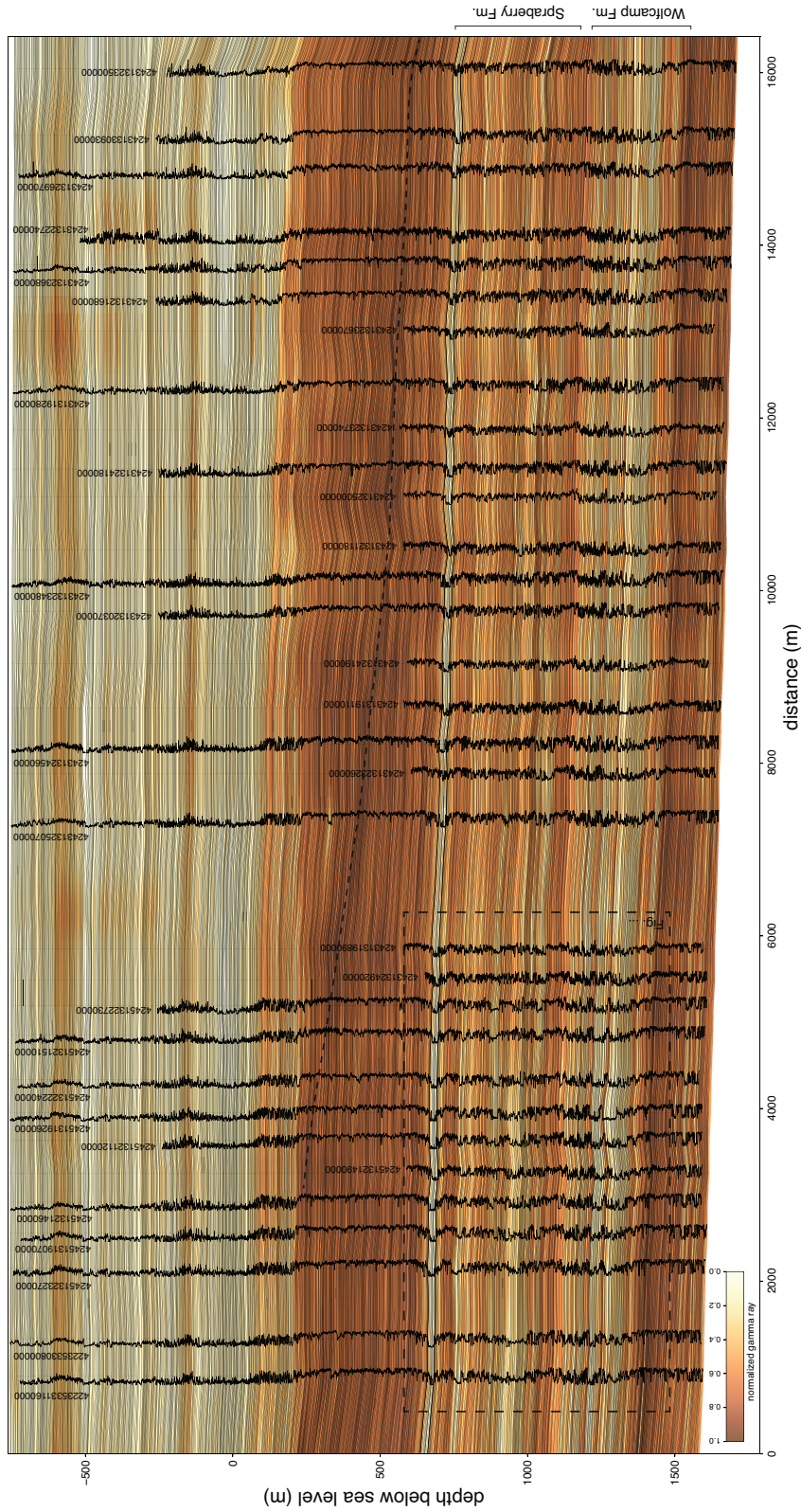


Figure 12: Dip section showing the shelf carbonates at the top, slope mudstones in the middle, and basal siliciclastics (Spraberry Fm.) and carbonates (Wolfcamp Fm.) at the base. See Fig. 18 for location of section.

3 CASE STUDY

To illustrate the potential of the workflow described above, we use a set of 681 gamma ray logs from the Permian Basin in West Texas. Processed versions of these logs are available in a [public data repository](#). The wells span three counties in

Texas: Sterling, Tom Green, and Irion counties, which are all located on the eastern side of the Midland Basin (Fig. 11). The wells in the study area penetrate Lower Permian rocks that include basinal carbonates of the Wolfcamp Formation at the bottom, siliciclastic deep-water units of the Spraberry Formation, and well-stratified shelf carbonates at the top. A mudstone-dominated unit separates the Spraberry Formation from the shelf carbonates; this interval shows clinof orm geometries in nearby seismic lines and are likely to have been deposited on the slope.

To determine which well pairs to correlate, we have used a maximum distance of 1500 m; this resulted in 9569 well pairs (Fig. 2d) that were correlated using the DTW algorithm with an exponent of 0.15. Only the gamma ray logs were used in the correlation; therefore, low-gamma-ray limestones and siltstones or sandstones are not distinguished in the figures that follow. At the highest resolution, the interval of interest was subdivided into 2585 stratigraphic units, using a wavelet width of 1. With a wavelet width of 4, the number of stratigraphic units is reduced to 1223; this was the scale that we relied on to generate a gridded model, with a cell size of 100 m x 100 m in the x- and y directions. This model was used to generate cross sections that capture well the stratigraphy.

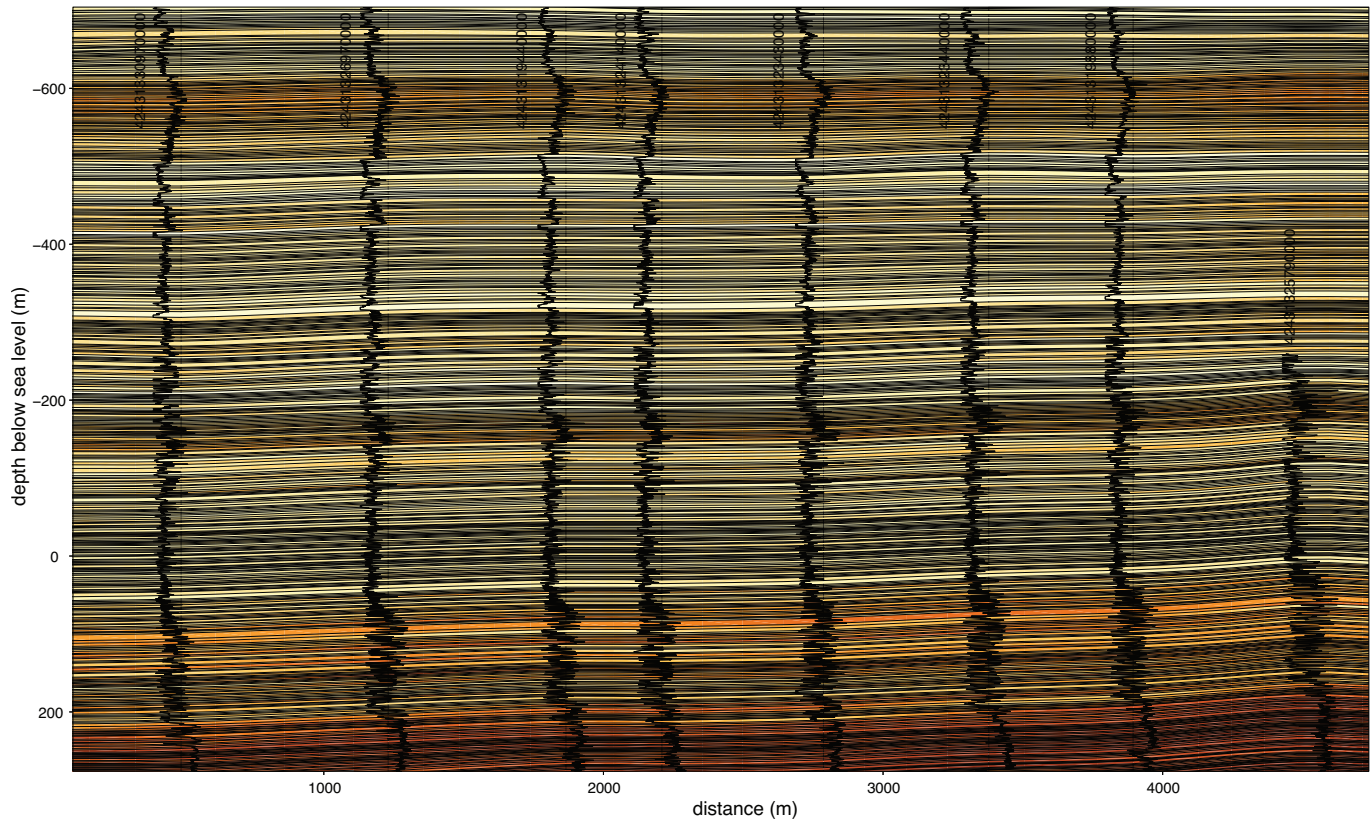


Figure 13: High-resolution correlation result from the well-layered carbonates at the top of the correlated section.

A dip section covering most of the area of interest illustrates well the mostly low gamma-ray basinal carbonates and siliciclastics at the bottom of the section (Fig. 12), the high-gamma-ray slope mudstones in the middle, and the shelf carbonates at the top. Apart from some lenses of more massive carbonates, especially on the western side of the section, these shelf carbonates are well layered and are correlated by ChronoLog at a high level of detail, with no obvious errors in the correlation results (Fig. 13). The lowermost layers of the shelf carbonates transition toward the basin into mudstones, illustrating the idea that this approach to correlation is not a simple lithologic correlation. The correlation surfaces within the slope mudstones are inclined relative to the basin- and shelf sediments below and above, suggesting that clinof orms are present in this interval. However, the true dip of the clinof orms is probably larger than that captured by ChronoLog. A vaguely defined low-gamma-ray unit (dashed lines in Figs. 8, 12) is a likely indication of what these true dips are. Despite the high well density, there is not enough signal in the well logs in this interval to get the steep dips, in part due to the fact that these mudstones are likely to contain channels and mass transport deposits. However, it is possible to manually interpret the surface in the chronostratigraphic diagram (Fig. 8) and use the interpretation to create an adjusted correlation framework. The quality of the correlations in the carbonate section above the slope mudstones improves significantly as a result (Fig. 14).

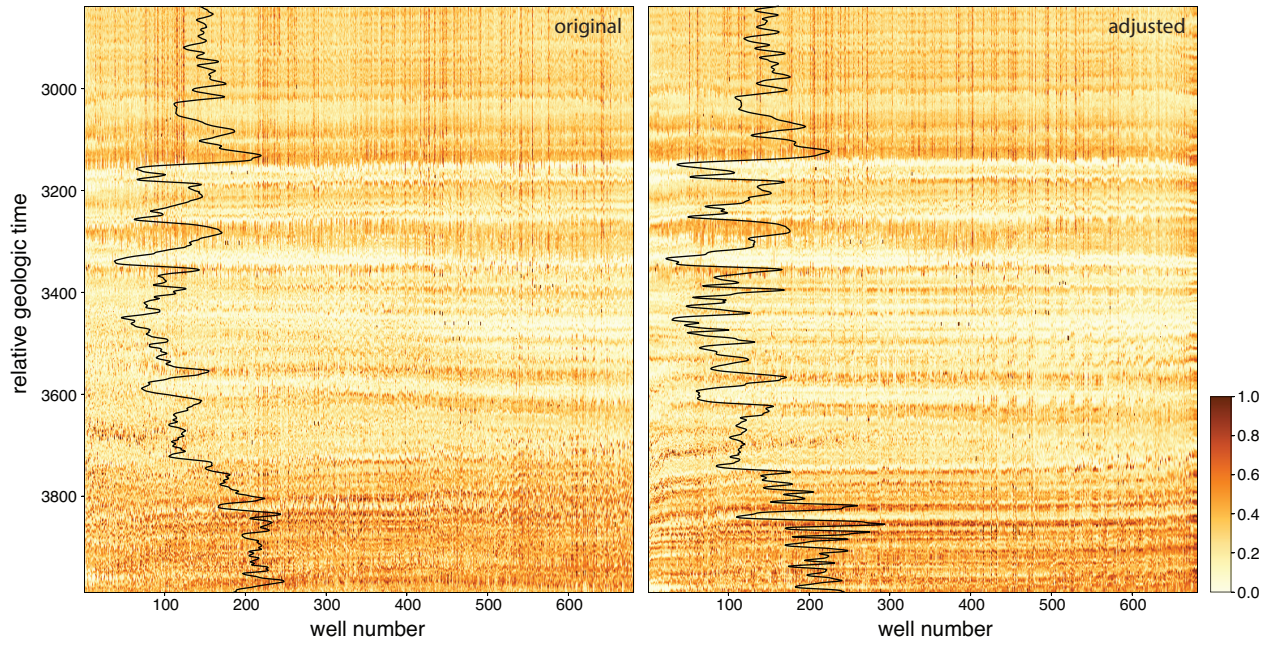


Figure 14: Detail of chronostratigraphic diagram before (left) and after (right) manual adjustment of the correlation result.

A laterally continuous low-gamma-ray unit is present at the top of the Spraberry Formation (Fig. 12). This apparent continuity is due to the fact that the cross section is following the axis of a linear basin-floor submarine channel, which is likely filled with siltstone and sandstone. Below this channel, the Spraberry Formation consists of laterally continuous, but gradually changing intervals, that are likely to be submarine lobes; the lowermost part of the formation is laterally more variable and is probably contains a significant number of slumps and mass-transport deposits. The lateral variability in the log character is more obvious in a zoomed-in version of the section (Fig. 15) that shows more detail. Both in this and the large-scale section, it is obvious that the Wolfcamp Formation is more laterally continuous and relatively easy to correlate.

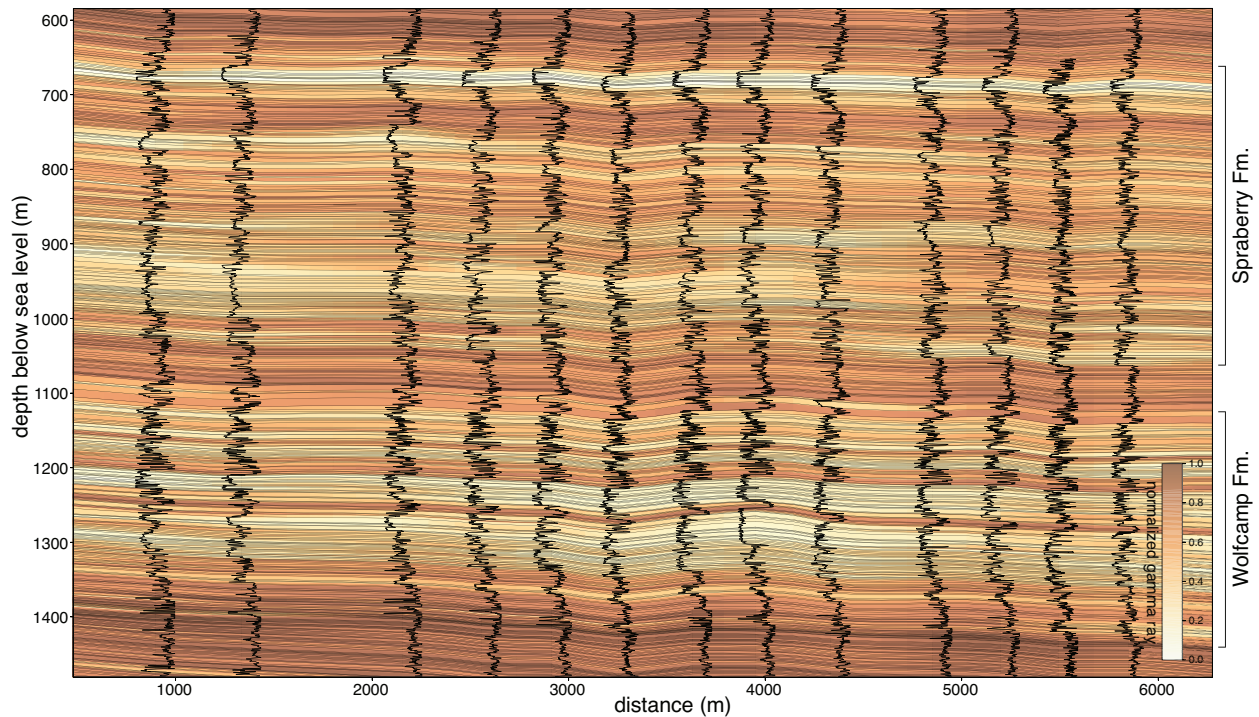


Figure 15: Detail of correlation result from the dip section in Fig. 12.

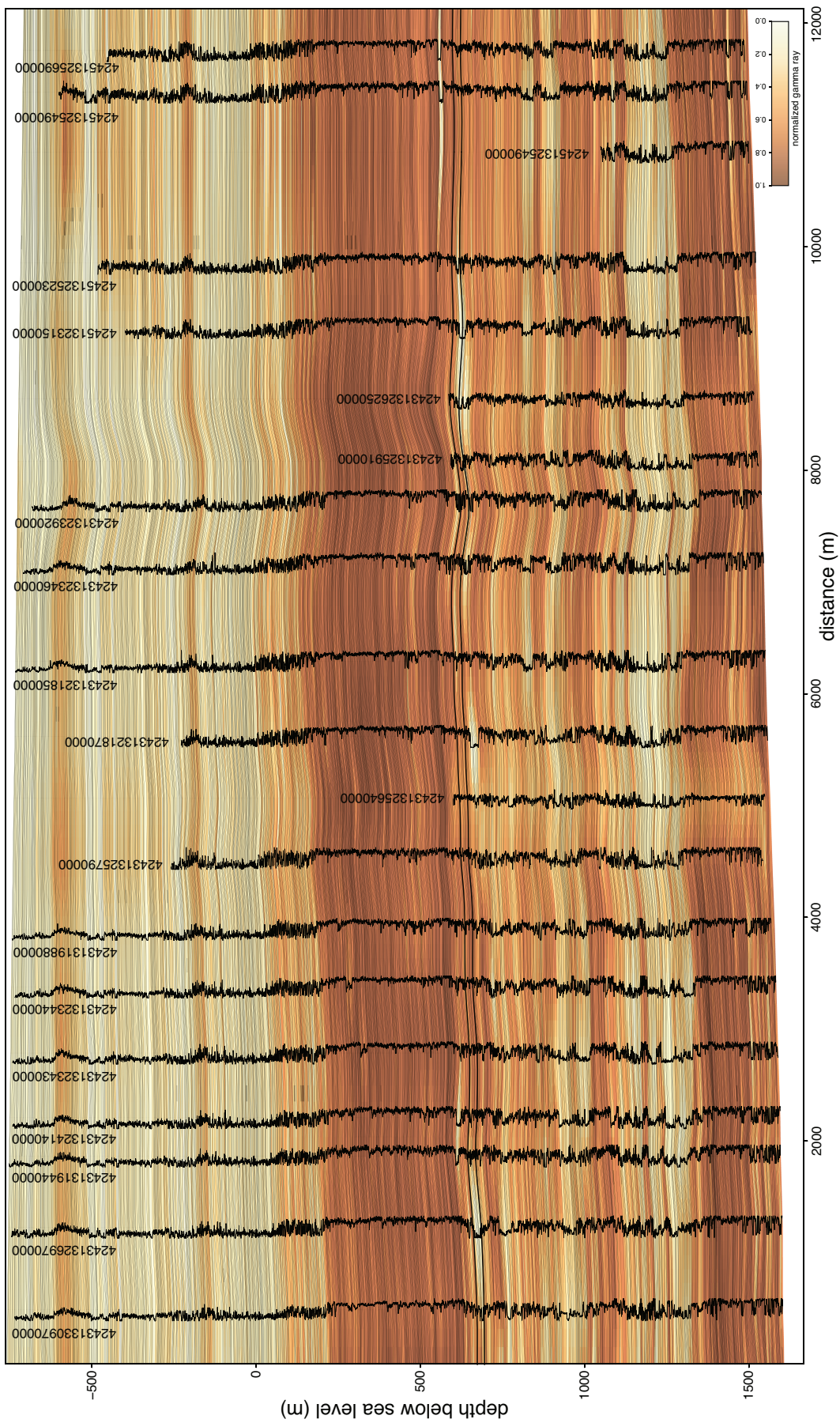


Figure 16: Strike section through a high-resolution correlation result. Lateral discontinuity in the uppermost part of the Spraberry Formation is due to the presence of submarine channels. Thicker black lines highlight the interval that was used to map the channels in Fig. 18.

The lenticular nature of the coarser-grained units in the Spraberry Formation is more obvious in strike sections (Figs. 16, 17). The channel fills in the upper part of the formation are 0.5-1 km wide and have a cleaner gamma-ray signature than the coarser-grained units below. The ChronoLog surfaces do not follow the bases of these channels; instead they enforce a layercake-like interpretation that suggests numerous facies transitions. As in the dip sections, there are no obvious correlation errors, unless some of these facies transitions are counted as such.

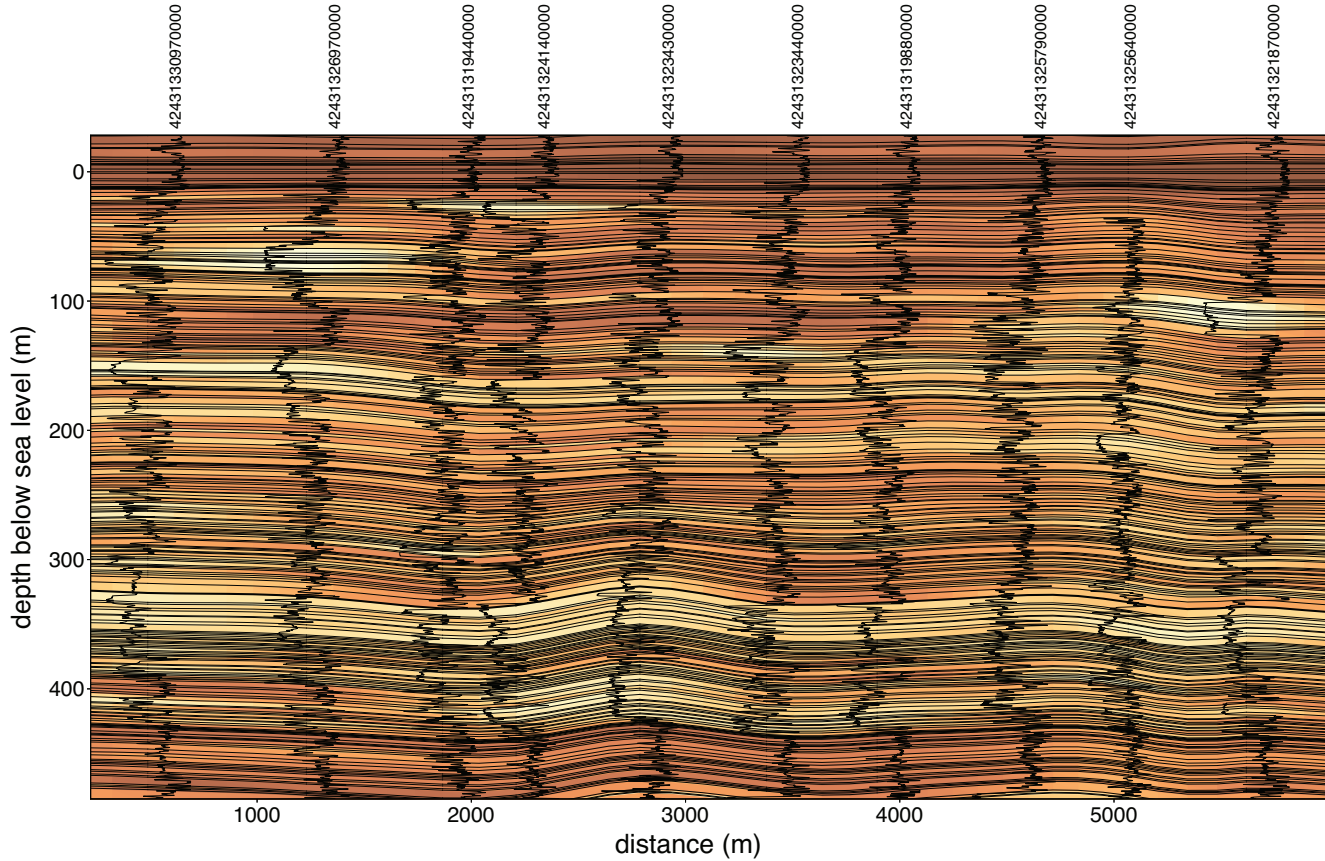


Figure 17: Detail of the strike section in Fig. 16, showing lateral variability in the Spraberry Formation.

The low-sinuosity channels of the upper Spraberry Formation are well expressed in average property maps that are created through averaging the log property between two stratigraphic tops (Fig. 18). They are relatively wide, low-sinuosity, close to linear features, with thicknesses of 10-30 m, probably similar to submarine channels described from outcrops of the Brushy Canyon Formation (e.g., Beaubouef et al., 1999). These channels are quite different from the highly sinuous and laterally mobile channels that are common on longer and taller passive-margin continental slopes (e.g., Deptuck et al., 2003, 2007; Deptuck and Sylvester, 2018).

4 DISCUSSION

A key element of our correlation approach is the dataset-wide optimization of the depth shifts, largely following the Wheeler and Hale (2014) method, so that a consistent three-dimensional stratigraphic framework can be built. As a result of this optimization, lateral facies changes are common in the correlation result. In addition, the output is far from what one could get from correlating based on lithologic similarity which is what the DTW well-pair correlation relies on. This is a major problem of manual correlation: when only looking at a cross section, it is difficult and subjective to avoid correlating based on lithologic similarity. A non-lithostratigraphic approach requires substantial knowledge of the nature and the scale of facies transitions in a variety of depositional environments and of the local geology. In contrast, the approach described here considers a large number of well pairs at the same time, in three dimensions, and automatically figures out what facies transitions are necessary to eliminate all the correlation conflicts.

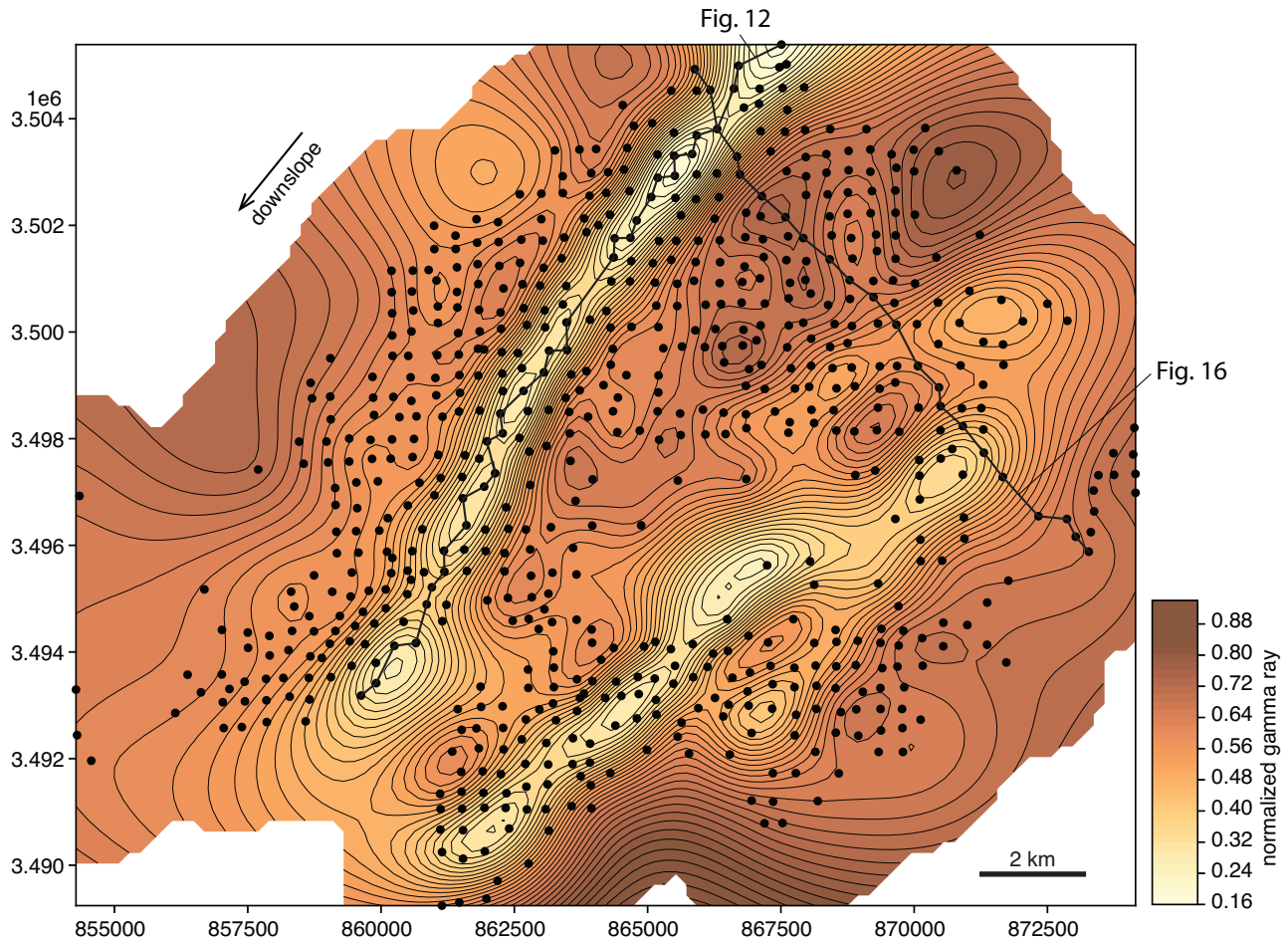


Figure 18: Map of normalized gamma-ray values of the uppermost part of the Spraberry Formation, outlining the fills of wide, low-sinuosity submarine channels.

However, this bias toward relatively simple layercake correlations, combined with the lack of any specific stratigraphic knowledge in the code also means that significant and large-scale stratigraphic surfaces such as onlaps, downlaps, and unconformities can be either unrecognized or poorly handled. For example, the onlap of Brushy Canyon Formation sediments onto slope mudstones of the northern Delaware Basin is commonly represented in ChronoLog outputs as a facies transition. This does not mean that all significant lateral thickness changes remain undetected. The presence of clinoforms was recognized in the slope mudstones of the Sterling County dataset (Fig. 12), even if it is likely that the real clinoforms are steeper. A dataset that includes the Sterling County well cluster used above but covers a larger area shows the potential of the ChronoLog approach to recognize and document clinoform geometries (Fig. 19).

At the scale of up to a few hundred meters, typical of inter-well distances in densely drilled areas, stratigraphy tends to be more variable than over scales of several kilometers. In fact, the pronounced variability that is often the focus of outcrop studies does not imply significant variability at the larger scale. Although it is tempting to try applying outcrop-scale observations in log correlation, it is unlikely that a more aggressive interpretation approach (e.g., one that could automatically detect erosional surfaces at the bases of channels) would be useful and successful. Even relatively simple and large channel bodies, like those in the upper part of the Spraberry Formation, are only mappable because their width exceeds the typical well spacing (Fig. 18). The majority of channels and other laterally highly variable stratigraphic elements are only penetrated by a small number of wells that are not enough to confidently detect and map those elements. Although often a lot of time is spent trying to manually paint in these features in cross sections, it is more practical to rely on a layercake correlation that is known to be incorrect in its details but is reproducible and reflects the uncertainty of how exactly the stratigraphic architecture looks like. However, it is important to keep in mind that, even with high well densities, ChronoLog outputs are more laterally continuous and simpler than the real stratigraphy.

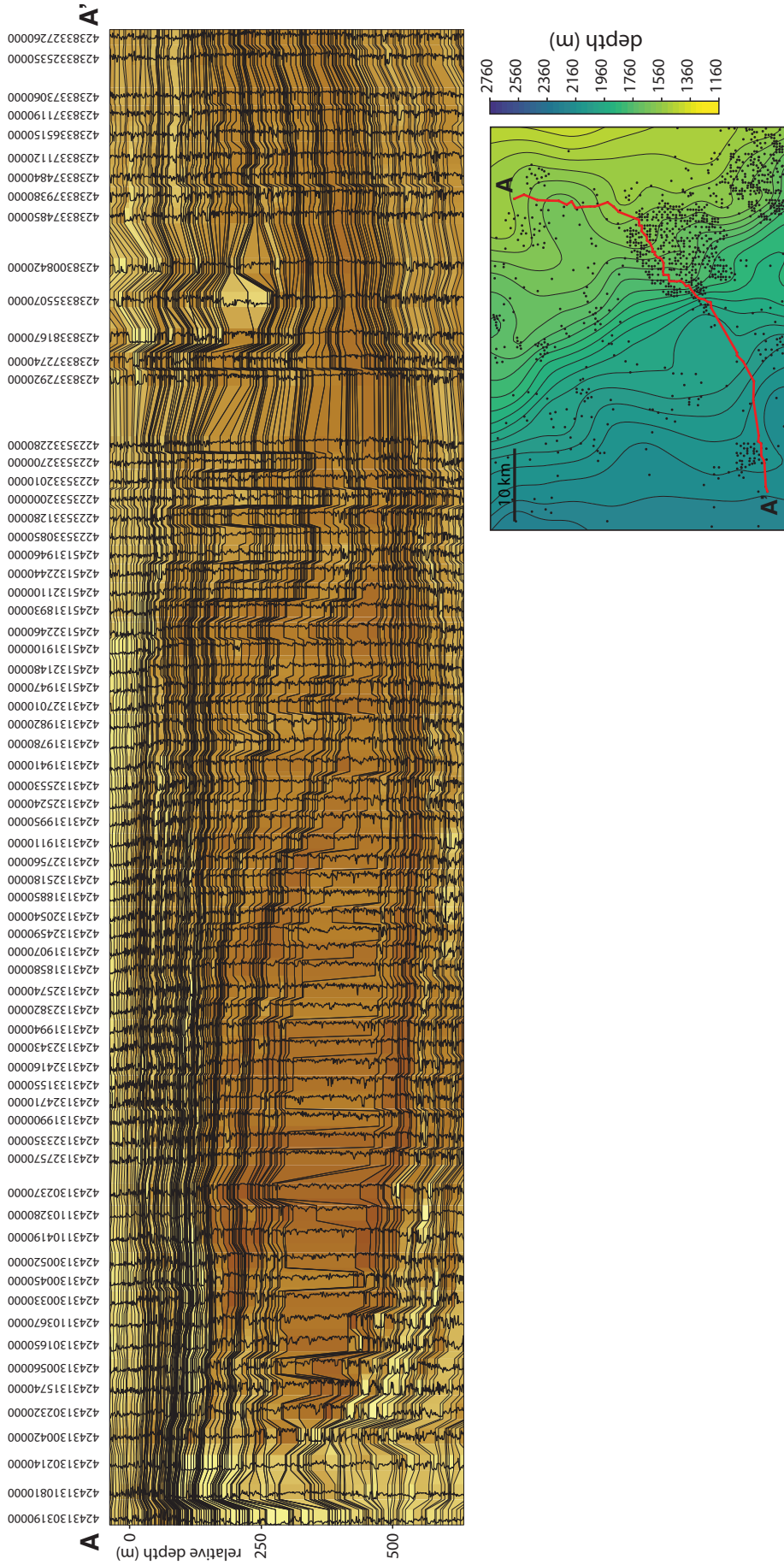


Figure 19: A large-scale NE-SW cross section from the eastern side of the Midland Basin, showing clinoforms captured in the ChronoLog correlation result.

A novel and important aspect of our log correlation approach is the creation and use of the chronostratigraphic diagram (Fig. 8). These diagrams give a quick, large-scale overview of the stratigraphy of the area and interval of interest. They can be used to quickly identify laterally continuous mudstones, stratigraphic units with significant internal variability, lateral facies transitions, and, maybe most importantly, intervals and locations where the correlation results could be improved. It is difficult to find correlation errors in conventional log correlation panels that were built using ChronoLog (Figs. 12, 13, 15, 16, 17) as often such errors are manifested through a gradual and subtle shift of correlation surfaces that is difficult to detect in neighboring logs. In contrast, projecting all the wells into a single section means that relatively distant logs can be displayed next to each other and errors become more obvious.

This raises the question whether such errors could be eliminated using the ChronoLog algorithm or an improved version of it. While improvements to the algorithm are certainly possible, in practice it is difficult to force the global optimization to improve a particular detail in the correlation. Instead, the chronostratigraphic diagrams themselves can be used to manually adjust the correlation results. One possibility is to select a well-defined stratigraphic marker, e.g., a laterally continuous mudstone, and pick it in every column / log of the chronostratigraphic diagram. Then the whole correlation process can be run separately on the log segments above and below this marker and a new, adjusted chronostratigraphic diagram can be assembled through stacking the two partial diagrams together. This approach makes sure that the marker surface is a timeline in the new chronostratigraphic diagram. Alternatively, we have also implemented a less precise but more time-efficient technique that allows the interpreter to quickly define an adjustment surface by drawing on the chronostratigraphic diagram (Fig. 8). The corresponding stratigraphic tops are estimated through interpolation; the endpoints of the drawn segments are extended across the remainder of the logs as constant values. For example, adjusting the Sterling County chronostratigraphic diagram by flattening one of the prominent clinoforms results in significant improvements of the correlation well above the adjusted marker (Fig. 14). It is obvious from the diagram that further improvements are possible ; in practice, the effort put into such improvements can be a function of how important is to get near-perfect results for a certain interval.

The multi-scale aspect of the ChronoLog workflow means that the resolution of the stratigraphic framework can be chosen as a function of the problem at hand. For example, it is computationally expensive if reservoir models used for simulating fluid flow have a large number of gridcells. Fine-scale geological models with a large number of layers often need to be coarsened to reduce the number of cells and ideally this coarsening is done so that key stratigraphic boundaries are preserved (e.g., Lie, 2019). The approach described here is designed to preserve the most important stratigraphic boundaries as one moves from a fine-scale subdivision of the stratigraphy to coarser layering (Fig. 20).

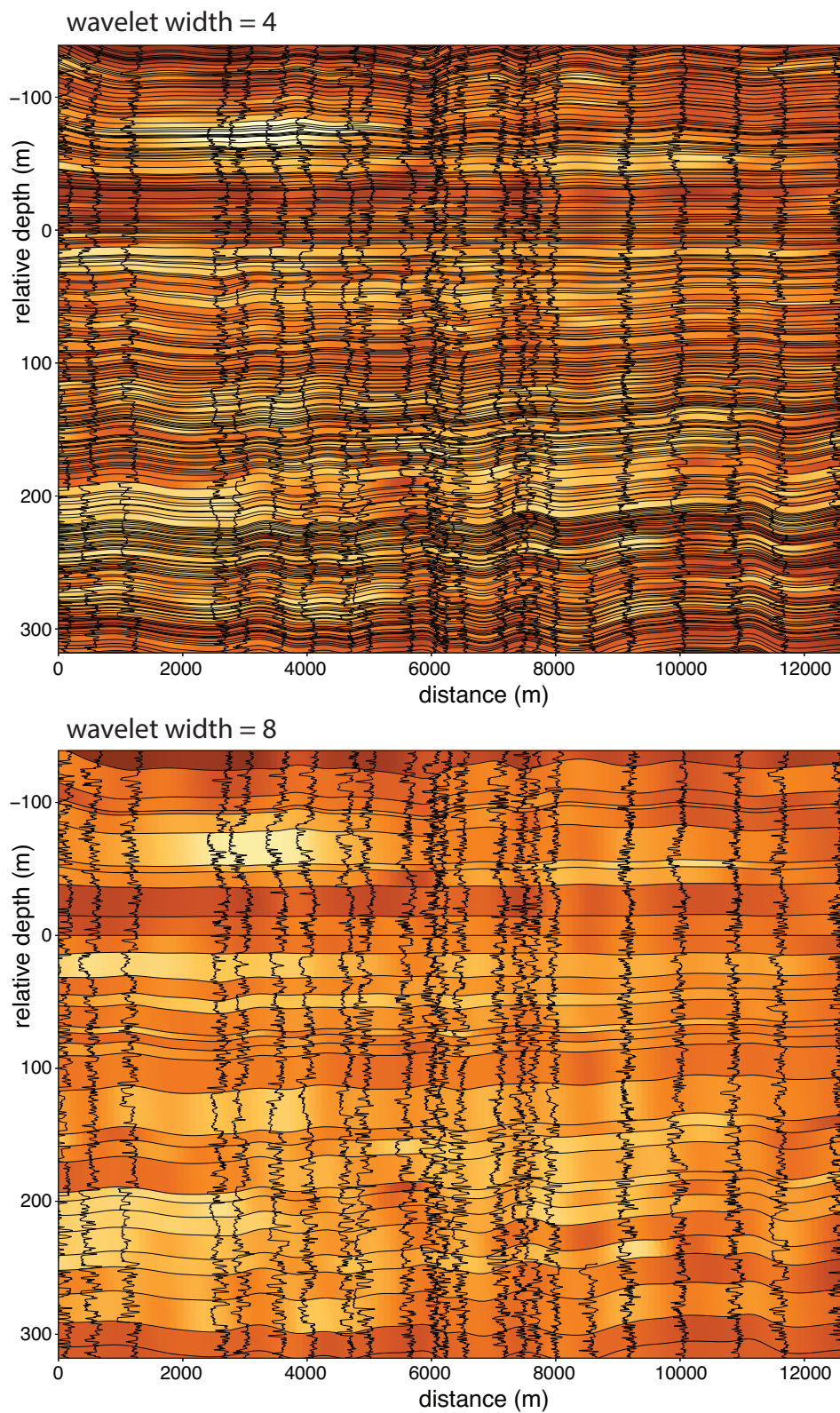


Figure 20: Cross sections through two stratigraphic models of different resolution, capturing the variability of the Spraberry Formation.

5 CONCLUSIONS

A multi-scale stratigraphic framework can be automatically constructed for datasets with a large number (at least a few tens) of geophysical well logs with relatively close spacing. Key elements of the approach presented here include (1) defining an overall top and base for the interval of interest and imputing missing log segments; (2) loading log data into a database in the form of a graph, with well objects as nodes and edges defining the log pairs that need to be correlated; (3) log pair correlation using the dynamic time warping algorithm, with a distance measure that reduces the influence of outliers; (4) transforming the logs into a chronostratigraphic diagram, with relative geologic time on the vertical axis, through computing the optimal depth shifts that minimize correlation errors; (5) using the continuous wavelet transform to define a stratigraphic hierarchy based on the mean log that was derived from the chronostratigraphic diagram; (6) converting RGT values that correspond to markers in different levels of this hierarchy back to depth; (7) building a three-dimensional stratigraphic model through gridding every stratigraphic interval at a certain scale; and (8) visualizing results as cross sections in which stratigraphic intervals are colored according to the mean log property.

The main advantage of this approach over conventional manual log correlation workflows - or automated techniques that focus on one top at a time - is that it quickly provides an overview of the large-scale stratigraphic structure, while also generating a large number of stratigraphic tops if high-resolution detail is of interest. The chronostratigraphic diagram is useful for detecting laterally persistent stratigraphic units and ones that are subject to facies transitions. It also highlights areas of problematic correlations, which then can be improved by manually interpreting the correct correlation in the diagram and re-running the correlations above and below this surface.

ChronoLog correlation results tend to be relatively simple, layer-cake style, without a lot of rapid thinning, thickening, and stratigraphic pinchouts. This means that lateral facies transitions and gradual changes in thickness are likely to be well handled. Depositional elements like channels and lobes commonly have laterally extensive time-equivalent deposits (Figs. 17, 20), and, as a result, they are not without context when viewed in property maps (Fig. 18). However, large-scale erosional- and onlap surfaces are likely to be misinterpreted as facies transitions; and further work is needed to improve the results in the presence of such surfaces.

Although here we have focused exclusively on geophysical well logs, the approach described here is likely to result in improved correlation frameworks for time series datasets where spatial position is relevant and the similarity of the time series is relatively high. For example, it has significant potential in correlating paleo-proxy records of environmental change, including various records from marine and lacustrine sediments (e.g., Hay et al., 2019; Ajayi et al., 2020), corals, ice cores, speleothems, tree rings, and varves. The potential for improvement over previous approaches that rely on dynamic time warping is that it considers a large number of log pairs and finds a solution that minimizes the conflicts between the resulting correlations.

6 ACKNOWLEDGEMENTS

This project would not be where it is today without numerous discussions with and help from Jacob Covault, Joan Gomberg, Margaret Murakami, Buddy Price, Xavier Janson, Zsófia Poros, Glennis Sylvester, Donny Keighley, Austin Bailey, Mark Holland, Matt Wolinsky, and Joseph Yeh. The well log data used in the study was derived from the S&P Global Permian Basin Digital Logs Subscription. Financial support for this work was provided the members of the Quantitative Clastics Laboratory research consortium (<http://www.beg.utexas.edu/qcl>) at the Bureau of Economic Geology, The University of Texas at Austin.

7 REFERENCES

- Ajayi, S., Kump, L.R., Ridgwell, A., Kirtland Turner, S., Hay, C.C., and Bralower, T.J., 2020, Evaluation of PaleoceneEocene Thermal Maximum Carbon Isotope Record CompletenessAn Illustration of the Potential of Dynamic Time Warping in Aligning PaleoProxy Records: *Geochemistry, Geophysics, Geosystems*, v. 21, doi:10.1029/2019GC008620.
- Baldwin, J., Otte, D.N., and Whealtley, C.L., 1989, Computer Emulation of Human Mental Processes: Application of Neural Network Simulators to Problems in Well Log Interpretation, Paper SPE-19619 presented at the SPE Annual Technical Conference and Exhibition, San Antonio, Texas, 811 October. DOI: 10.2118/19619-MS.
- Brazell, S., Bayeh, A., Ashby, M., and Burton, D., 2019, A Machine-Learning-Based Approach to Assistive Well-Log Correlation: *Petrophysics*, v. 60, p. 469479, doi:10.30632/PJV60N4-2019a1.
- Cooper, G.R.J., and Cowan, D.R., 2009, Blocking geophysical borehole log data using the continuous wavelet transform: *Exploration Geophysics*, v. 40, p. 233, doi:10.1071/EG08127.
- de Bruin, G., Hemstra, N., and Pouwel, A., 2007, Stratigraphic surfaces in the depositional and chronostratigraphic (Wheeler-transformed) domain: *The Leading Edge*, v. 26, p. 883-886, doi:10.1190/1.2756868.
- Deptuck, M.E., Steffens, G., Barton, M.D., and Pirmez, C., 2003, Architecture and evolution of upper fan channel-belts on the Niger Delta slope and in the Arabian Sea: *Marine and Petroleum Geology*, v. 20, p. 649676, doi:10.1016/j.marpetgeo.2003.01.004.

- Deptuck, M.E., Sylvester, Z., Pirmez, C., and O Byrne, C., 2007, Migration-aggradation history and 3-D seismic geomorphology of submarine channels in the Pleistocene Benin-major Canyon, western Niger Delta slope: v. 24, p. 406433, doi:10.1016/j.marpetgeo.2007.01.005.
- Deptuck, M. and Sylvester, Z., 2017, Submarine Fans and Their Channels, Levees, and Lobes, In *Submarine Geomorphology*, Springer International Publishing, p. 273299, doi: 10.1007/978-3-319-57852-1_15.
- Fang, J.H., Chen, H.C., Shultz, A.W., and Mahmoud, W., 1992, Computer-Aided Well Log Correlation: AAPG Bulletin, v. 76, p. 307317.
- Grant, C.W., Bashore, W.M., and Compton, S., 2018, Rapid Reservoir Modeling with Automated Tops Correlation, in *Proceedings of the 6th Unconventional Resources Technology Conference*, Houston, Texas, USA, American Association of Petroleum Geologists, doi:10.15530/urtec-2018-2904037.
- Hagberg, A., Swart, P., and S Chult, D., 2008, Exploring network structure, dynamics, and function using networkx, in Report Number LA-UR-08-05495, Los Alamos National Lab. (LANL), Los Alamos, NM (United States), <https://www.osti.gov/biblio/960616>.
- Hamlin, H. S., and Baumgardner, R. W., 2012, Wolfberry (Wolfcampian-Leonardian) Deep-Water Depositional Systems in the Midland Basin: Stratigraphy, Lithofacies, Reservoirs, and Source Rocks: The University of Texas at Austin, Bureau of Economic Geology, Report of Investigations No. 277, 61 p.
- Harris, C.R. et al., 2020, Array programming with NumPy: Nature, v. 585, p. 357362, doi:10.1038/s41586-020-2649-2.
- Hay, C. C., Creveling, J. R., Hagen, C. J., Maloof, A. C., and Huybers, P. (2019). A library of early Cambrian chemostratigraphic correlations from a reproducible algorithm. *Geology*, v. 47(5), p. 457460, doi:0.1130/G46019.1.
- Hladil, J., Vondra, M., Cejchan, P., Vich, R., Koptikova, L., and Slavik, L., 2010, The dynamic time-warping approach to comparison of magnetic-susceptibility logs and application to Lower Devonian calciturbidites (Prague Synform, Bohemian Massif): *Geologica Belgica*, v. 13, p. 385406.
- Hunter, J.D., 2007, Matplotlib: A 2D Graphics Environment: Computing in Science & Engineering, v. 9, p. 9095, doi:10.1109/MCSE.2007.55.
- Jones, E., Oliphant, T., and Peterson, P., 2001, SciPy: Open Source Scientific Tools for Python, <http://www.scipy.org>.
- Kiusalaas, J., 2013, *Numerical Methods in Engineering With Python 3*, Cambridge University Press, 423 p.
- Kluyver, T., Ragan-Kelley, B., Pérez, F., Granger, B.E., Bussonnier, M., Frederic, J., Kelley, K., Hamrick, J.B., Grout, J., Corlay, S. and Ivanov, P., 2016, Jupyter Notebooks-a publishing format for reproducible computational workflows, in: Loizides, F. and Schmidt, B. eds., *Positioning and Power in Academic Publishing: Players, Agents and Agendas: Proceedings of the 20th International Conference on Electronic Publishing*, Yektaweb Publishing Company, p. 8790, doi:10.3233/978-1-61499-649-1-87.
- Lallier, F., Caumon, G., Borgomano, J., Viseur, S., Fournier, F., Antoine, C., and Gentilhomme, T., 2012, Relevance of the stochastic stratigraphic well correlation approach for the study of complex carbonate settings: application to the Malampaya buildup (Offshore Palawan, Philippines): *Geological Society, London, Special Publications*, v. 370, p. 265275, doi:10.1144/SP370.12.
- Lallier, F., Caumon, G., Borgomano, J., Viseur, S., Royer, J.-J., and Antoine, C., 2016, Uncertainty assessment in the stratigraphic well correlation of a carbonate ramp: Method and application to the Beausset Basin, SE France: *Comptes Rendus Geoscience*, v. 348, p. 499509, doi:10.1016/j.crte.2015.10.002.
- Lie, K.-A., 2019, *An Introduction to Reservoir Simulation Using MATLAB*, Cambridge University Press, 392 p.
- Lineman, D.J., Mendelson, J.D., and Toksöz, M.N., 1987, Well-to-Well Log Correlation Using Knowledge-Based Systems and Dynamic Depth Warping:, <http://dspace.mit.edu/handle/1721.1/75091>.
- Lisiecki, L.E., and Lisiecki, P.A., 2002, Application of dynamic programming to the correlation of paleoclimate records: *Paleoceanography*, v. 17, p. 1-12, doi:10.1029/2001PA000733.
- Lisiecki, L., and Raymo, M., 2005, A Pliocene-Pleistocene stack of 57 globally distributed benthic $\delta^{18}O$ records: *Paleoceanography*, v. 20, p. 1-17, doi:10.1029/2004PA001071.
- Lomask, J., Francis, J., Rickett, J., Buursink, M., Gerber, T., Perlmutter, M., and Paola, C., 2009, New tools for seismic stratigraphic interpretation: Stratal convergence and instantaneous isochron attribute cubes derived from volumetric flattening of experimental strata: v. 93, p. 453459.
- Luthi, S.M., and Bryant, I.D., 1997, Well-log correlation using a back-propagation neural network: *Mathematical Geology*, v. 29, p. 413425, doi:10.1007/BF02769643.
- Mann, C.J., and Dowell, T.P.L., 1978, Quantitative lithostratigraphic correlation of subsurface sequences: *Computers & Geosciences*, v. 4, p. 295306, doi:10.1016/0098-3004(78)90064-X.

- McFee, B., Raffel, C., Liang, D., Ellis, D., McVicar, M., Battenberg, E., and Nieto, O., 2015, librosa: Audio and Music Signal Analysis in Python, Proceedings of the 14th Python In Science Conference, Austin, Texas, p. 1824, doi:10.25080/Majora-7b98e3ed-003.
- Oliphant, T.E., 2006, Guide to Numpy, 378 p.
- Qayyum, F., Catuneanu, O., and Groot, P., 2014, Historical developments in Wheeler diagrams and future directions: Basin Research, p. 115, doi:10.1111/bre.12077.
- Rudman, A. J., and Lankston, R. W., 1973, Stratigraphic Correlation of Well Logs by Computer Techniques: AAPG Bulletin, v. 57, p. 577-588, doi:10.1306/819A4306-16C5-11D7-8645000102C1865D.
- Uieda, L., 2018, Verde: Processing and gridding spatial data using Greens functions: Journal of Open Source Software, v. 3, p. 957, doi:10.21105/joss.00957.
- Virtanen, P. et al., 2020, SciPy 1.0: fundamental algorithms for scientific computing in Python: Nature Methods, v. 17, p. 261272, doi:10.1038/s41592-019-0686-2.
- Wheeler, L., and Hale, D., 2014, Simultaneous correlation of multiple well logs, in SEG Technical Program Expanded Abstracts 2014, Denver, Colorado, Society of Exploration Geophysicists, p. 618622, doi:10.1190/segam2014-0227.1.
- Wheeler, L.F. Automatic and simultaneous correlation of multiple well logs: M.S. Thesis, Colorado School of Mines, 40 p.
- Wu, X., Shi, Y., Fomel, S., and Li, F., 2018, Incremental correlation of multiple well logs following geologically optimal neighbors: Interpretation, v. 6, p. T713T722, doi:10.1190/INT-2018-0020.1.
- Wu, X., Li, Y., and Sawasdee, P., 2022, Toward accurate seismic flattening: methods and applications: Geophysics, p. 137, doi:10.1190/geo2021-0662.1.
- Zoraster, S., Paruchuri, R. K., and Darby, S., 2004, Curve Alignment for Well-to-Well Log Correlation, SPE Annual Technical Conference and Exhibition, Houston, Texas, doi: <https://doi.org/10.2118/90471-MS>.